A LASER TECHNIQUE FOR CALIBRATION OF PIEZOELECTRIC TRANSDUCERS USED TO MEASURE UNDERWATER SHOCK PRESSURES

C. E. Edlund
G. F. Munsch
P. J. Pantermuehl
B. W. Vanzant

FINAL REPORT
Contract N00014-66-C0318
SwRI Project 03-1933

Prepared for
Field Projects Branch
Office of Naval Research
Washington, D. C.

July 1971

SOUTHWEST RESEARCH INSTITUTE
SAN ANTONIO HOUSTON

Unclassified

Security Classification

DOCUMENT CONTROL DATA - R & D

(Security classification of title, body of abstract and indexing annotation must be entered when the overall report is classified)

1. ORIGINATING ACTIVITY *(Corporate author)*
Southwest Research Institute
P.O. Drawer 28510
San Antonio, Texas 78228

2a. REPORT SECURITY CLASSIFICATION
Unclassified

2b. GROUP
N.A.

3. REPORT TITLE

A LASER TECHNIQUE FOR CALIBRATION OF PIEZOELECTRIC TRANSDUCERS USED TO MEASURE UNDERWATER SHOCK PRESSURES

4. DESCRIPTIVE NOTES *(Type of report and inclusive dates)*
Final Report

5. AUTHOR(S) *(First name, middle initial, last name)*

C. E. Edlund P. J. Pantermuehl
G. F. Munsch B. W. Vanzant

6. REPORT DATE	7a. TOTAL NO. OF PAGES	7b. NO. OF REFS
July 1971	75	22

8a. CONTRACT OR GRANT NO.	9a. ORIGINATOR'S REPORT NUMBER(S)
N00014-66-C-0318	03-1933 Final Report
b. PROJECT NO.	
c.	9b. OTHER REPORT NO(S) *(Any other numbers that may be assigned this report)*
d.	

10. DISTRIBUTION STATEMENT

11. SUPPLEMENTARY NOTES	12. SPONSORING MILITARY ACTIVITY
	Office of Naval Research Arlington, Virginia 22217

13. ABSTRACT

A crossed beam laser Dopplermeter was used to measure particle velocity at an explosively generated shock front in water. The shock front velocity was measured by detecting the time interval required for the shock front to intersect two parallel laser beams a known distance apart. A tourmaline piezoelectric gage was positioned at the same distance from the explosive charge as was the point of intersection of the crossed beam system. The peak shock overpressure as indicated by the tourmaline transducer was the same as that calculated by the product of front velocity times particle velocity times density of the undisturbed water. Although the system is marginal for measuring particle velocity with existing equipment, it is anticipated that normal technological advances will eventually permit such a system to be used to calibrate underwater shock transducers.

DD FORM 1 NOV 65 1473

Unclassified

Security Classification

14 KEY WORDS	LINK A		LINK B		LINK C	
	ROLE	WT	ROLE	WT	ROLE	WT
Laser applications						
Interference and diffraction						
Dopplermeter						
Laser interferometer						
Underwater particle velocity measurement						
Underwater shock						
Underwater shock front velocity measurement						

SOUTHWEST RESEARCH INSTITUTE
Post Office Drawer 28510, 8500 Culebra Road
San Antonio, Texas 78284

A LASER TECHNIQUE FOR CALIBRATION OF PIEZOELECTRIC TRANSDUCERS USED TO MEASURE UNDERWATER SHOCK PRESSURES

C. E. Edlund
G. F. Munsch
P. J. Pantermuehl
B. W. Vanzant

FINAL REPORT
Contract N00014-66-C0318
SwRI Project 03-1933

Prepared for
Field Projects Branch
Office of Naval Research
Washington, D. C.

July 1971

Approved:

Robert C. DeHart, Director
Department of Structural Research

TABLE OF CONTENTS

LIST OF FIGURES

LIST OF FIGURES (Cont'd)

LIST OF FIGURES (Cont'd)

I. INTRODUCTION

Calibration of piezoelectric pressure transducers intended for use in measuring shock pressure generated by an explosion is usually accomplished in what may be termed a "backwards" manner: the transducer is immersed in a cylinder of liquid which is pressurized to a desired level and suddenly depressured at one end by means of a quick-release mechanism. This causes a pressure relief wave of known magnitude and description to be transmitted into the cylinder. The time history of the pressure pulse impinging on the transducer is experimentally repeatable and mathematically predictable. Piezoelectric response of the transducer can then be related to the known magnitude of this shock pressure. The calibrating pulse is, however, one with a pressure decrease across the propagating front. When the transducer is placed in an environment influenced by an underwater explosion, it will experience a propagating front with a pressure increase, the reverse of the calibrating pulse.

It is conceivable that more accuracy could be obtained by using a calibration technique entailing evaluation of the fundamental parameters necessary to describe the phenomenon of pressure differential across a shock front. The pressure rise across a shock front may be expressed as[1]

$$p = c_o \rho_o \dot{u} \left[1 + \frac{2\dot{u}}{c_o}\right] \qquad (1)$$

where p = pressure rise across the front #/ft^2
ρ_o = density of fluid prior to arrival of pressure disturbance #/sec^2/ft^4
c_o = shock front velocity, ft/sec
$\dot{u}$ = velocity of particles at shock front, ft/sec

For low magnitude shocks of less than 1 Kbar the particle velocity, $\dot{u}$, is small relative to the acoustic velocity, c_o, and the bracket in Equation (1) reduces to unity. Consequently, Equation (1) reduces to

$$p = c_o \rho_o \dot{u} \qquad (2)$$

Thus the fundamental parameters of shock pressure are the velocity with which the disturbance propagates, the density of the medium into which it is propagating and the velocity imparted to the particles due to the passage of the front. To determine the value of a shock pressure at a point, it is necessary to measure the front and particle velocities at that point while the front is passing; the density of the undisturbed fluid can be predetermined.

From the preceding definition of shock overpressure, it was conceived that a laser Dopplermeter could be used to measure the velocity of particles at the shock front, while the front velocity was simultaneously being monitored, thereby providing a probeless technique to measure free field shock overpressures. The laser Dopplermeter compares the frequency of laser radiation scattered from moving particles in a fluid with the primary or fundamental frequency generated by the laser. The difference between the frequencies, as explained by the Doppler effect, is a measure of the velocity of particles in the fluid. Several investigators[2, 3] have used this method to study continuous flow distribution under both laminar and turbulent conditions.

Although the Dopplermeter method is readily applicable for monitoring continuous flow, its application for monitoring the transient signal produced by a shock front traversing the sensing region imposes several problems not encountered with continuous flow. First, the shock front is characterized by a rapid change in particle velocity occurring over a very thin region. To detect and faithfully reproduce such a phenomenon requires a wide bandwidth system. Obtaining an adequate signal to noise ratio is thus more difficult than in the case of continuous flow measurements, where narrow bandwidth can be used to advantage in reducing the effective level of noise. A second difficulty is encountered due to the nature of the signal which is composed of a very rapid change in Doppler frequency occurring over a very short time interval. Measurement of the frequency content of such a nonrecurring signal poses several problems, such as insuring that all the apparatus is adjusted for optimum performance at the instant the shock wave crosses the sensing region.

During the course of the study, several Dopplermeter systems having various limitations were experimentally investigated before a successful system evolved. The following describes the systems used and summarizes the results obtained.

II. TECHNICAL DISCUSSION

A. Laser Radiation

The well publicized advantages of light from a laser over the light from other sources are due to the spatial and temporal coherence of the laser radiation.[4] The spatial coherence makes possible the well-defined beam which exhibits little spreading and which may be focused to a very high degree. Typical divergence figures for a gas laser are on the order of 0.7 milliradian which permits the transmission over large distances with comparatively little loss in intensity. It also allows the power in the beam to be concentrated into a very small volume to produce an extremely high power density. In the proposed system, this characteristic permits the sensing region to be sufficiently small that spatial resolution can be at least an order of magnitude better than that now achieved with pressure transducers.

The frequency (or temporal) coherence of laser radiation is the characteristic which determines both the width of the band in which the emission is concentrated and the stability of this band. While the radiation from ordinary monochromatic sources can be used to produce interference phenomena when two light paths of the same length are combined, the effect is not observable over paths of significantly different lengths. The much higher coherence of laser radiation allows similar phenomena to be observed over light path lengths of much greater difference in lengths. The narrower frequency speed of laser radiation also allows measurement of time rate of change of path lengths to be observed for much lower velocities than is possible with ordinary light sources.

In the initial part of the program, a Spectra Physics Model 119 helium-neon continuous wave laser was used. This laser emits only a single line with very high stability characteristics. The specified performance characteristics of this laser result in a single line emission of 62328°A with a power of 100 microwatts. It was necessary to use this single mode device in the pure Dopplermeter system as it was originally conceived. Problems in the signal to noise ratio due to the low power level necessitated trying other systems in which the single mode characteristic was not essential. Consequently, a Spectra Physics Model 124 He Ne laser with a 15 milliwatt output was used in later experiments. Although this laser had seven major modes with 214 Mhz spacing, the multiple modes did not have a deleterious effect on the systems in which it was used.

B. Phenomena of Scattered Radiation

If radiation from a source of light is directed into a small fluid volume, δV, most of the light will be transmitted through the region, but a small portion will be scattered by the molecules of the medium and any suspended particles. Light scattering is a well-known phenomena which has been classically treated in two categories: those of Rayleigh, and Mie. The ratios of incident to scattered intensities in either case are dependent on essentially the same parameters; however, their functional dependence differs. Rayleigh scattering, which is applicable to the case of scattering by particles much smaller than the wavelength of the light, is defined by the relation

$$\frac{I_s}{I_o} = N(\delta V)\left(\frac{2\pi}{\lambda}\right)^4 \frac{a^2}{R^2} \cdot \frac{1}{2} (1 + \cos^2 \phi) \qquad (3)$$

where

I_s - intensity of scattered light

I_o - intensity of incident light

N - number of scattering particles per unit volume, cm^{-3}

δV - scattering volume element, cm^3

λ - wavelength of incident radiation, cm

R - distance from δV, cm

a - polarizability of the scattering particles, cm^3

ϕ - angle between R and the incident beam

The Mie scattering relation is applicable to scattering from particles comparable to and greater than the wavelength of the light and is given, after Penndorf[5] as $dI = -I_o \pi R^2 KN$. The ratio of intensities, as before, may be written as

$$\frac{I_s}{I_o} = \ell \pi R^2 NK \qquad (4)$$

where

ℓ - scattering length of a unit diameter

I_0 - intensity of incident beam

N - number of scattering particles per unit volume

R - scattering particle radius

K - dimensionless total Mie scattering coefficient

The amount of radiation arriving at the particle velocity detector due to Mie scattering from impurities in the water, such as dust particles, rust, etc., contributes to the particle velocity Doppler signal and can, in fact, provide the majority of the scattered intensity unless the water is quite pure. If tests confirm that small impurity particles on the order of 1 to 2-micron diameter follow the water particle velocity, then their presence may be deemed an asset in that the dynamic range of this measurement technique can be made greater due to the increase in the light level at the detector the additional scattered light provides.

C. Reflection and Refraction of Radiation

While measurements of the particle velocities depend on scattering of light from a region, measurements of the shock front velocity depend on a reflection (or refraction) of a laser beam at the interface of the front and the propagation medium. To determine the feasibility of measurements based on this phenomena, an estimate of the intensity of the reflected signal is required.

The relation, $R = \left[(n - 1)/(n + 1)\right]^2$, gives the reflectivity, at normal incidence, of an optical interface whose relative index of refraction is n. The Lorentz-Lorenz relation

$$n = \frac{P_o}{\beta} \frac{(n_o^2 - 1)(n_o^2 + 2)}{6n_o} \qquad (5)$$

gives the refractive index of a media as a function of the pressure P_o, the optical media's bulk modulus β, and the standard refractive index of the media n_o. For a 6,000 psi peak overpressure shock, these relations indicate a shock front reflectivity of the order $R \sim 10^{-4}$. The theoretical value of this reflectivity coefficient has been substantiated by several investigators.[6,7] For a 100 microwatt incident laser beam, the total power in the shock front reflected laser image will be on the order of $P_R \sim 10^{-8}$ watt for radiation impinging on the front at normal incidence. This power level, while very small, is well within the capability of available photomultiplier detectors.

Reflections at an oblique angle, as used in the proposed system, are expected to be somewhat greater than those for a reflection normal to the front.

D. The Doppler Effect

The Doppler effect is well known for its usefulness in providing a basis for the precise determination of the velocity of moving objects. The phenomenon of the Doppler shift, as it pertains to electromagnetic radiation, is a direct consequence of the invariance of the velocity of light. It manifests itself as an apparent change in the frequency of radiation emanating from a given source if there is relative motion between the source and the observer. For the case under consideration, fluid in the volume δV will be in motion due to the arrival of a pressure disturbance. The detector will receive radiation scattered from this region and will indicate that it has a different frequency from the original laser signal. To a good approximation, the Doppler difference in frequency, due to motion in the region Δf, can be expressed as:

$$\Delta f = \frac{[K_o - K_s] \cdot \dot{u}}{2\pi} \tag{6}$$

where

K_o - number of cycles per unit length of incident beam, cm^{-1}

K_s - number of cycles per unit length of scattered radiation, cm^{-1}

$\dot{u}$ - velocity of the scattering volume, cm/sec

Δf - difference in frequency, sec^{-1}

$\dot{u}$ is a velocity vector, and $K_o - K_s$ is a wave vector. A schematic of a typical Dopplermeter system for which Equation (6) is applicable is shown in Figure 1. Since absolute values are of interest in numerical computations using data obtained from the system shown in Figure 1, it is convenient to rewrite Equation (6) as

$$\Delta f = \frac{2N\dot{u}}{\lambda_o} \sin\frac{\phi}{2} \sin\left(\psi + \frac{\phi}{2}\right) \tag{7}$$

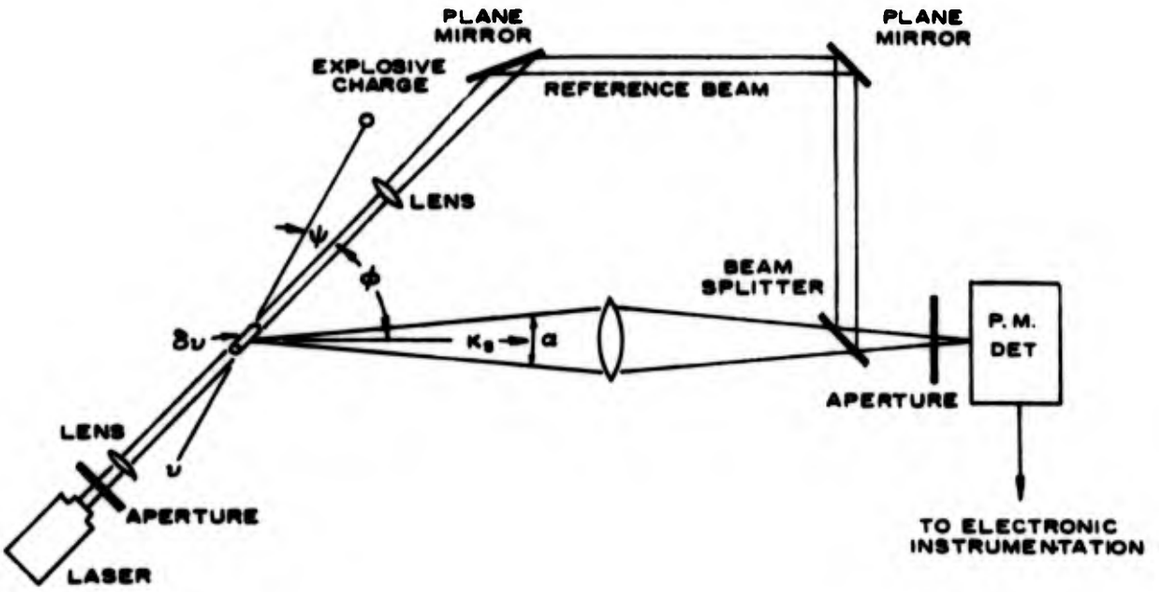

FIGURE 1. HOMODYNE DETECTION SYSTEM

where

N - refractive index of the fluid

λ_o - wavelength of incident radiation, cm

ϕ, ψ - angles dependent upon geometry as defined in Figure 1

For an He-Ne gas laser emitting radiation at a wavelength of 6328 Å, Equation (7) reduces to

$$\Delta f = 4.21 \times 10^4 \dot{u} (\sin \phi/2) \left[\sin (\psi + \phi/2)\right] \quad (8)$$

and for $\psi = 5°$, $\phi = 10°$ in Figure 1, the expression simplifies to

$$\Delta f = 637 \dot{u} \quad (9)$$

Using Equation (2) to determine the particle velocity due to the passage of a 6,000 psi shock overpressure, it is seen from Equation (9) that the Doppler difference frequency should be about 168 kilocycles. It is to be noted that all wave vectors generated with the solid angle $\mathscr{S}$ will be detected, but, if the selected angle is kept sufficiently small, the spread in geometry and velocities can be kept sufficiently narrow so that the accuracy will not be appreciably degraded.

E. Homodyne System

The system for particle velocity measurement shown in Figure 1 utilizes the shift in frequency of the incident radiation by any motion of the scattering particles. By knowledge of the geometry of the optical path and of the magnitude of the Doppler shift, it is possible to determine the particle velocity in the direction of the shock front.

A portion of the direct laser radiation, as well as radiation scattered from the fluid volume of interest, is directed into a sensitive photomultiplier type detector. The output signal is a voltage proportional in amplitude to the intensity of the light and of a frequency of the two inputs. Measurement of the frequency of the output voltage provides information on the Doppler shift due to the velocity of the particles in the scattering region.

The random particle movement as well as instabilities present in the laser radiation source, in the propagating medium, and in the mechanical structure of the optical system all cause the frequency difference between

the direct and scattered radiation to be spread over a band rather than being a single, discrete line. For this reason, the method of frequency measurement must be selected to be appropriate for this type signal.

The desired output of the frequency measuring system is a voltage proportional to frequency which may be read out on an oscilloscope. The readout presentation will be a time history of the particle velocity in the region of interest δV and should appear somewhat similar to the pressure-time trace produced by a shock front acting on a pressure transducer. The height of the trace excursion will be a measure of the particle velocity and consequently an indication of the overpressure.

Several investigators[2, 8, 9] have demonstrated the feasibility of measuring localized liquid and gas streaming velocities with an optical Doppler technique. They have also shown the usefulness of a Doppler system for observing the velocities of moving diffuse reflectors. In particular, the findings of Yeh and Cummins[2, 8] provide experimental support for the practicality of using a laser beam and the associated Doppler effect induced by the motion of fluid in a discrete region to measure the velocities of particles in that region. While their work is in the range of very low velocities, the reported data on frequency broadening of scattered radiation due to diffusion and linear translation of scattering centers imply that this measurement technique is limited by acoustic velocities as an upper bound and a few millimeters per second as a lower bound.

The optical components used in the system, including the laser, are commercial components. The system assembly was optimized for scattering studies in water, particularly for high particle velocities. Selected types of photomultiplier type detectors provide adequate sensitivity to detect the available scattered light intensity, though better performance in this portion of the system would ease the requirements imposed on some of the other items. The electronic amplifiers and frequency detection system required for the system were developed and periodically optimized for this application.

Figure 1 shows a Homodyne Doppler detection system. The reference frequency is the same as the original laser radiation frequency, so that zero velocity produces zero frequency output (DC). When the velocity increases from zero to the anticipated value, the output frequency rises from zero to the value determined by the geometry of the system. In order to accurately recover transient information from an AC signal, it is necessary that the following relation[11] be satisfied

$$F_c > 2f_m \tag{10}$$

where

F_c - instantaneous AC frequency

f_m - highest frequency component of the information to be detected

The highest frequency, f_m, can be derived from the rise time of the transient[12] by the relation

$$f_m = \frac{1}{2t_r} \tag{11}$$

where

t_r - rise time

Therefore, the instantaneous AC frequency of the Doppler signal should be no lower than 1 MHz for a rise time of 1 microsecond. In early experiments it became obvious that the homodyne system would be limited by commercially available components, so that alternative systems were considered.

F. Heterodyne Systems and Bragg Cell

A system using a reference frequency which differs from the frequency applied to the scattering region is called a Heterodyne system. The methods of producing the necessary offset which were considered included the use of a second laser which was locked to the existing one by a servo loop, and a mechanical modulator applied to the reference beam. The initially selected approach used an ultrasonic modulator, or Bragg cell, located in the reference beam. In order to produce an operating margin above the minimum requirement of 1 MHz for a rise time of one microsecond, 5 MHz was chosen as a lower limit for the offset frequency.

The Bragg cell consists of a transparent medium in which an ultrasonic wave is propagated at right angles to the optical path.[13] The ultrasonic wave interacts with the light beam in a manner similar to a moving diffraction grating, producing an output beam which is deflected from the original beam by the Bragg angle, as indicated in Figure 2 and shifted in frequency by the frequency of the ultrasonic modulation.

In order to produce true Bragg modulation, it is necessary that the ultrasonic beam be wide enough for a given light ray traversing the medium

at the Bragg angle to cross at least one full wavelength of the ultrasonic wave. To satisfy this condition, and the previously established minimum frequency, a 29.5 MHz transducer which produces a 9-mm diameter beam was selected. The Bragg cell was constructed of an aluminum block 25 mm x 25 mm x 75 mm with two holes drilled through at right angles, as shown schematically in Figure 2 and assembled in Figure 3. The transducer was installed in one end of the hole down the long axis, and an acoustic absorber filled the other end of this hole. The lateral passage was fitted with glass windows, and the cell was filled with water and sealed. The window openings were kept as small as possible to minimize electrical radiation from within the cell leaking out and reaching the detector and associated electronics. Since the two beams existing from a Bragg cell diverge, it is possible to remove the through beam and pass only the Bragg beam by proper location of an aperture. The transducer was excited by a well-shielded 29.5 MHz source which has an output capability of up to three watts. Operation at a level above approximately two watts produced cavitation and localized heating and density changes in the water in the Bragg cell, limiting the percentage of light which could be diffracted from the original beam. However, the Bragg beam produced was still several orders of magnitude higher in intensity than the scattered light, producing satisfactory mixing at the photomultiplier cathode when both beams were applied simultaneously. The Heterodyne system using the Bragg cell is shown schematically in Figure 4.

With the reference beam offset from the laser frequency by 29.5 MHz, the mixing of the scattered radiation and the modified reference beam produced an output of 29.5 MHz under quiescent conditions in the region of observation, rather than the zero frequency produced by the Homodyne system. Depending on the geometry of the system, a particle velocity which produces a 100 kHz Doppler frequency will change the frequency difference between the two beams to either 29.4 or 29.6 MHz. With the geometry shown in Figure 1, the frequency shift is upward to 29.6 MHz.

In order to recover the information as a difference in light frequencies, it was necessary to use a detector to convert the optical information into electrical signals to be applied to a suitable readout device. The RCA 4463 photomultiplier tube selected as a detector has the sensitivity and bandwidth necessary to accomplish the desired detection. The scattered light has the lowest intensity and was used to establish the maximum sensitivity requirements. From Equation (3), the ratio of intensities for pure Rayleigh scattering is on the order of 10^{-9}. From laboratory observations, the use of tap water instead of distilled water improved this ratio approximately two orders of magnitude without inordinately broadening the scattered Doppler signal. Using the laser output specification of 100 microwatts, the scattered light captured by the lens in the scattered beam should be on

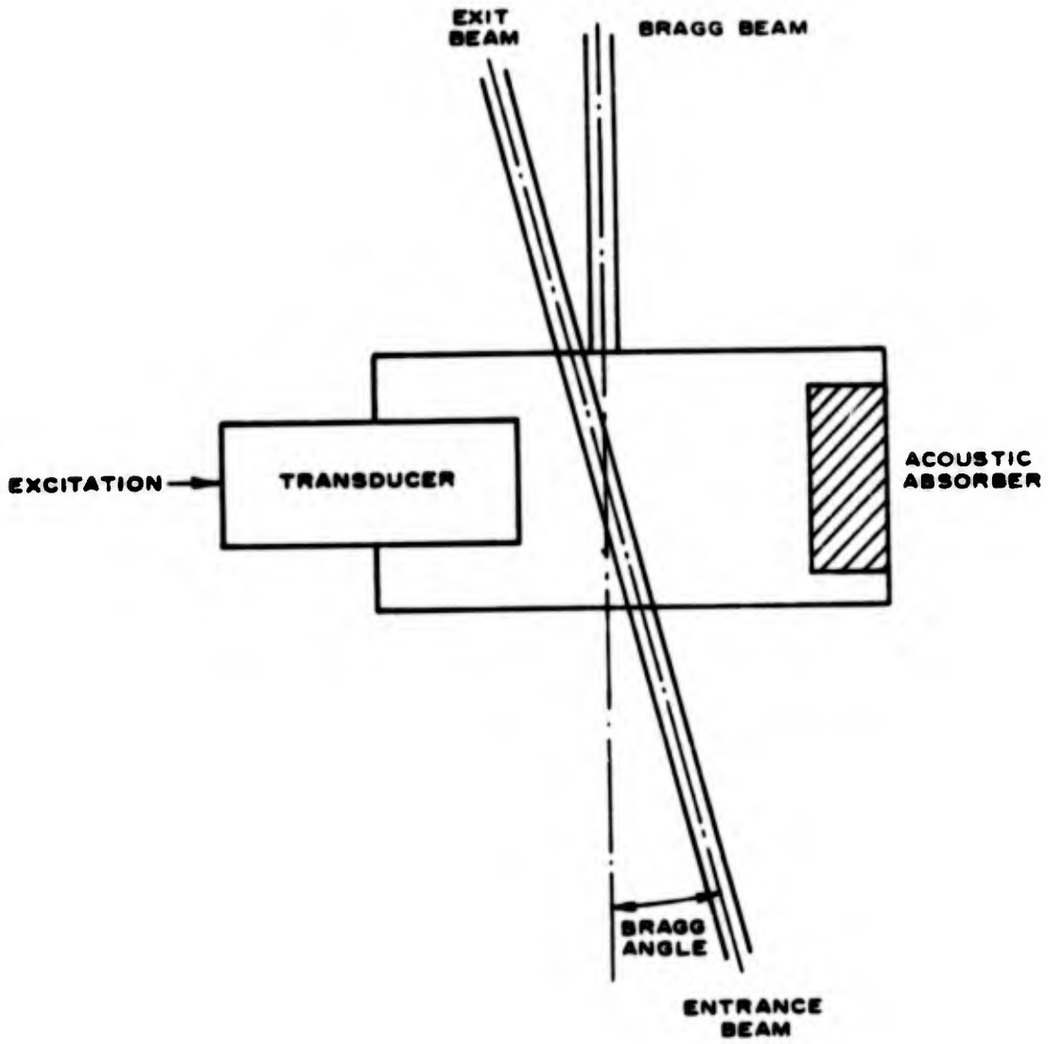

FIGURE 2. BRAGG CELL DETAIL

C-28639

FIGURE 3. BRAGG CELL ASSEMBLY

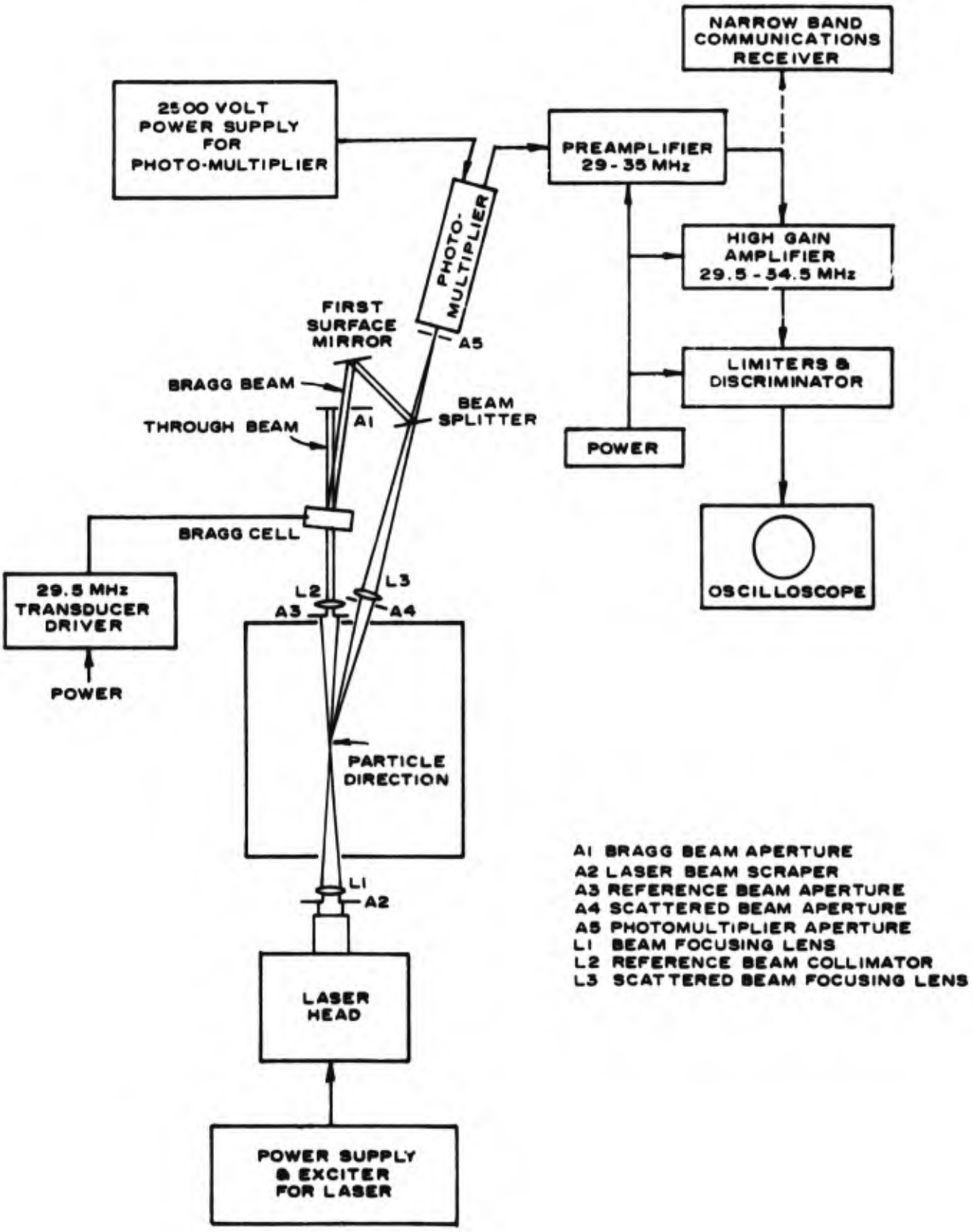

FIGURE 4. HETERODYNE SYSTEM WITH BRAGG CELL

the order of 10^{-11} watt. The typical characteristics of the photomultiplier give a radiant sensitivity of 2,100 amperes per watt. Thus, the output will be on the order of 2.1×10^{-8} ampere, which produced 1.05 microvolts across 50 ohms. To provide the frequency response required for Heterodyne detection, it was necessary that the RC time constant be shorter than the period of the output wave. This criterion was satisfied by a 50-ohm load resistance, which also matched the standard input impedance of amplifiers in this frequency range. With this information, the maximum bandwidth of the detector electronics could be calculated in order to preserve a usable signal to noise ratio. The general equation for equivalent noise input to an amplifier is

$$e_n^2 = 4kTRB \tag{12}$$

where

e_n - equivalent noise voltage

k - Boltzmann's constant = 1.374×10^{-23} joule per °K

R - resistance

T - absolute temperature °K

B - bandwidth

For a 1:1 signal to noise ratio, e_n is 1 microvolt, and, using the 50-ohm input resistance, the resulting bandwidth was 1.25 MHz. This bandwidth allows rise time measurements on the order of 0.4 microsecond, from Equation (11). Since a 1:1 signal to noise ratio is not sufficient to produce a satisfactory output signal to noise ratio in a standard FM detector, attempts to increase the signal to ratio to 2:1 were made by introducing scattering particles to increase the scattering intensity ratio by a factor of two.

G. Crossed Beam System

An alternative approach, equivalent to the Doppler model, has been described theoretically by M. J. Rudd[14]. The arrangement of this alternative system is shown schematically in Figure 5. The photomultiplier was focused on the point of beam intersection, P, which is the point of measurement.

The geometry of the interference pattern at the point of intersection is shown in Figure 6, with the pattern created by the nodal points of the fringes being shown in the enlargement. From this it can be seen that the minimal time for a particle to cross two fringes is

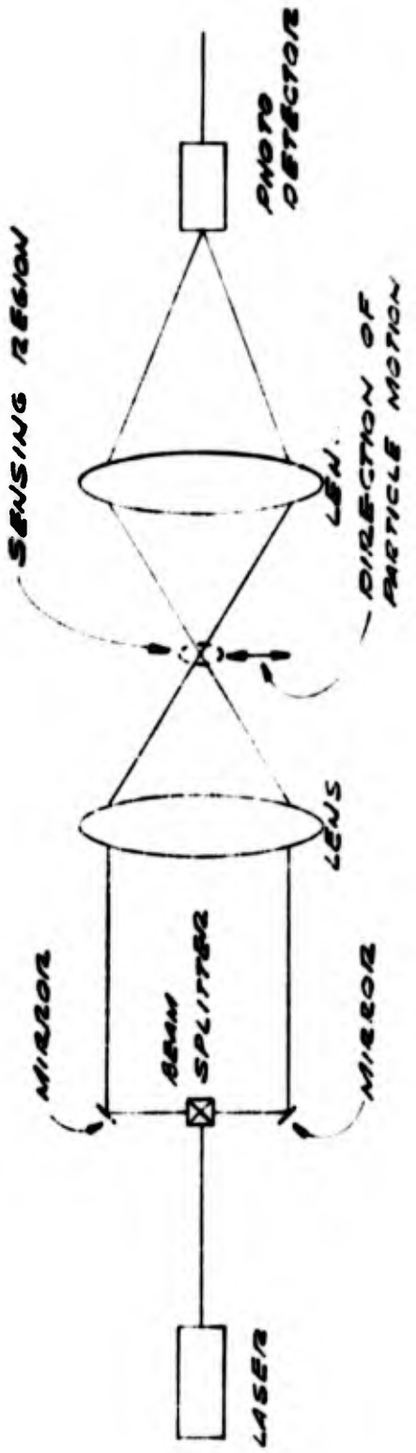

FIGURE 5. CROSSED BEAM SYSTEM

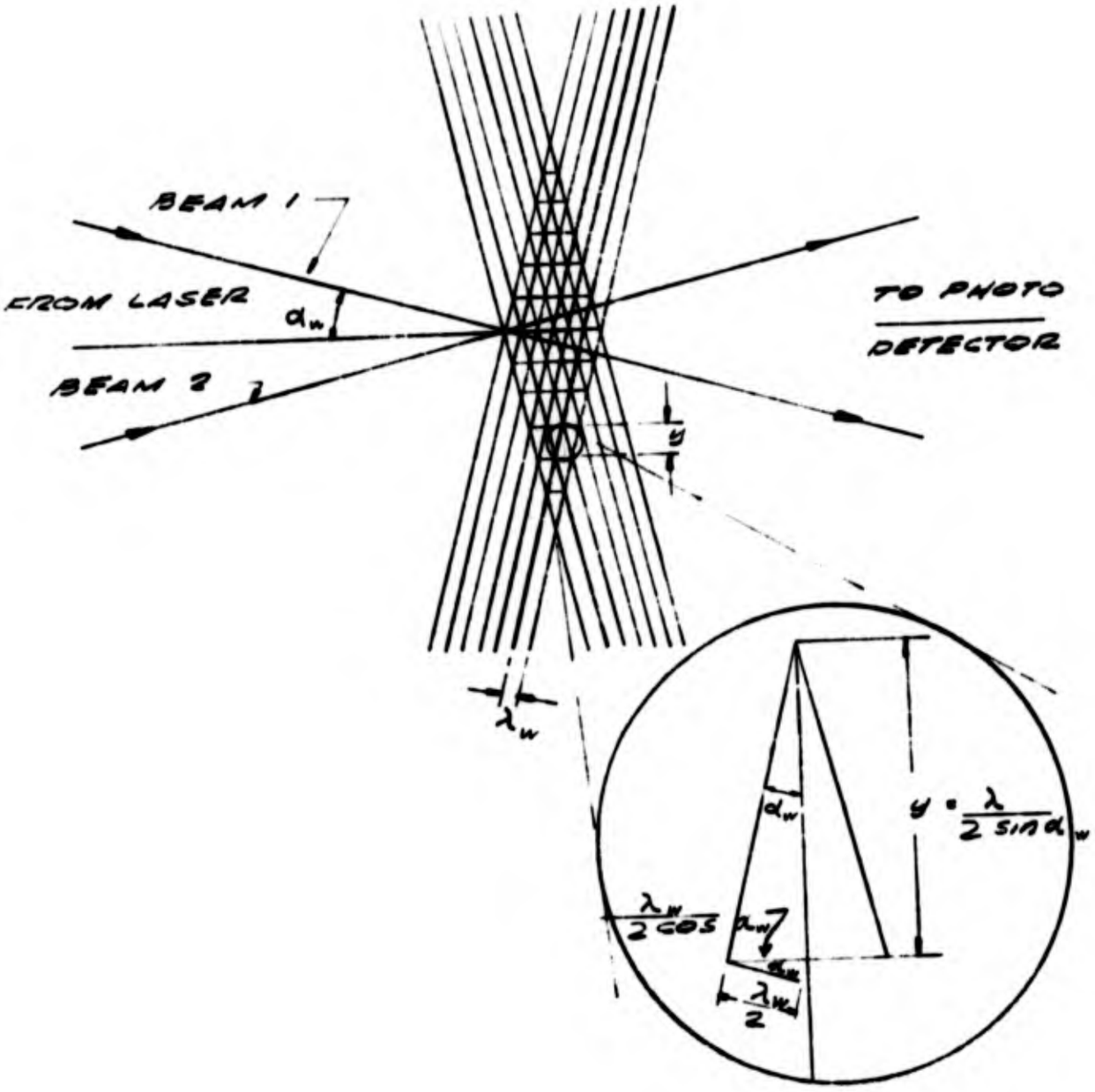

FIGURE 6. GEOMETRY OF BEAM INTERFERENCE

$$y = \frac{\lambda_w}{2 \sin \alpha_w} \tag{13}$$

where

y - distance between fringes

λ_w - wavelength of light being used (in water)

$2\alpha_w$ - angle between beams in water

n_w - refractive index for water

It is convenient to measure 2α in air rather than in water. According to Snell's law

$$n_o \sin \alpha_o = n_w \sin \alpha_w \tag{14}$$

where

n_o - refractive index for air $\cong$ unity

$2\alpha_o$ - angle between beams in air

Also,

$$\frac{\sin \alpha_o}{\sin \alpha_w} = n_w = \frac{v_o}{v_w} \tag{15}$$

where

v_o - velocity in air

v_w - velocity in water

But,

$$v_w = f\lambda_w \tag{16}$$

and

$$v_o = f\lambda_o$$

where

λ_o - wavelength of light in air

f - frequency

That is, when light goes from one medium to another its frequency remains constant but its wavelength changes as does its velocity. From Equations (15) and (16)

$$n_w = \frac{\lambda_o}{\lambda_w}$$
$$\lambda_w = \frac{\lambda_o}{n_w} \qquad (17)$$

Thus, Equation (13) may be written

$$y = \frac{\lambda_o}{2\, n_w \sin \alpha_w} \qquad (18)$$

From Equation (14)

$$\sin \alpha_w = \frac{\sin \alpha_o}{n_w} \qquad (19)$$

so that Equation (18) may be written as

$$y = \frac{\lambda_o}{2 \sin \alpha_o} \qquad (20)$$

which permits the angle to be measured outside of the explosive containment chamber.

As a particle crosses the region of fringes, a frequency change is produced at the photodetector which is proportional to the rate at which the fringes are being crossed. The relation between Doppler shift frequency and particle velocity is

$$\Delta f = f_d = \frac{\dot{u}}{y} \qquad (21)$$

where

f_d = Doppler shift frequency

Substituting from Equation (20)

$$f_d = \frac{2 \dot{u} \sin \alpha_o}{\lambda_o} \tag{22}$$

which is the fundamental equation relating particle velocity and Doppler shift frequency for the crossed beam system.

The validity of this expression was checked experimentally by splitting the radiation from the laser into two beams and rotating a disc (sprayed with 15 micron aluminum particles and clear lacquer) at the point of beam intersection. The disc was rotated at 1,000 rpm in such a way that the particles would move at right angles to the fringes at a radius of about 1.55 inches. The angle of beam intersection was varied. Results from this series of experiments are shown in Figure 7.

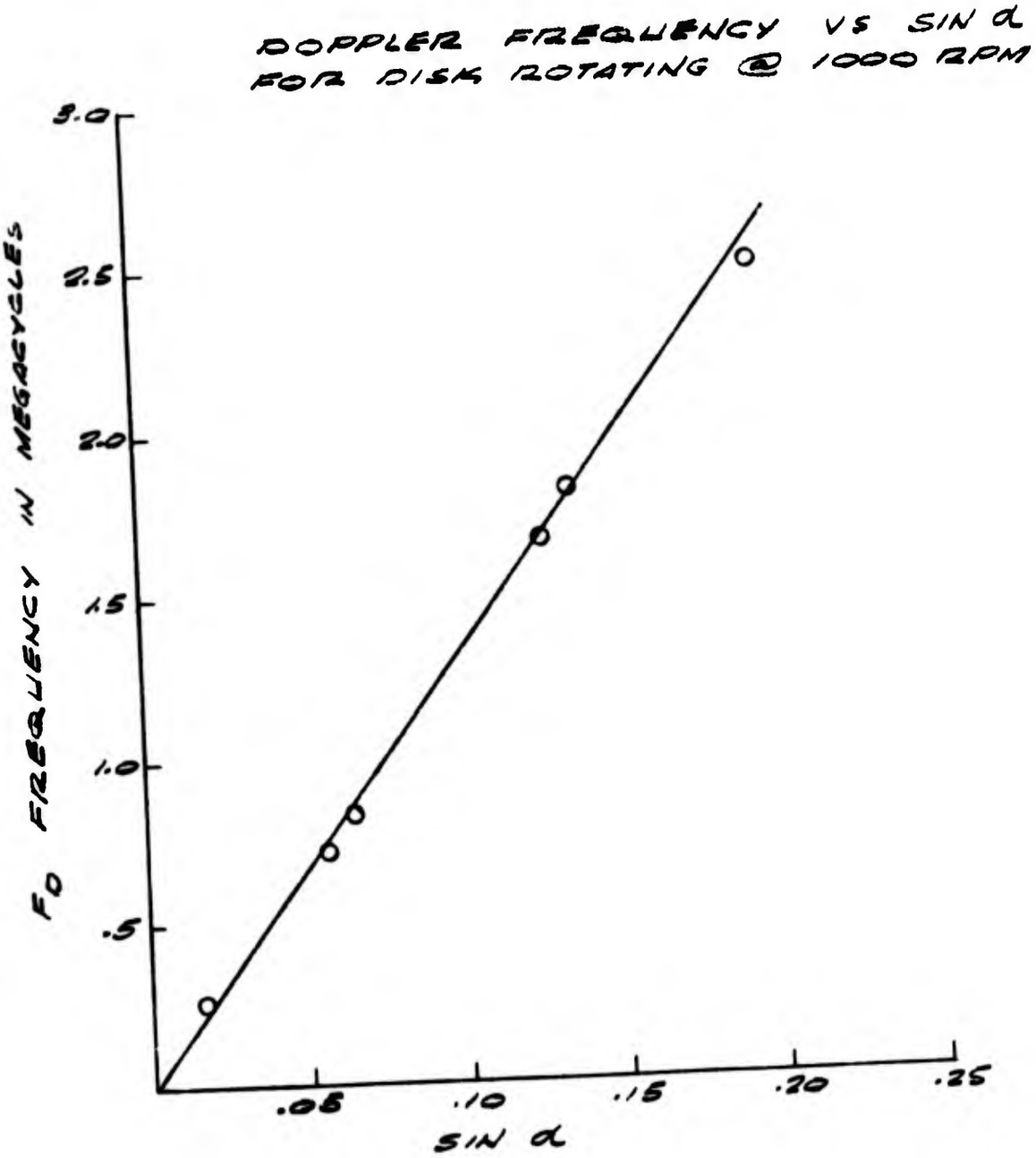

FIGURE 7. DOPPLER SHIFT FREQUENCY AS A FUNCTION OF BEAM ANGLE

III. EXPERIMENTAL PROCEDURE AND RESULTS

A. Homodyne System

Initial experimental efforts were concentrated on perfecting a system to measure steady state or constant velocity flow with a homodyne system. After considering various published comments[15-19] on optimization of particular portions of a Doppler system, the system shown schematically in Figure 8 was assembled.

The laser selected for this initial effort was a Spectra-Physics Model 119 which was considered at the time to be the only laser with the spectral and temporal coherence necessary to perform Doppler measurements over the total path length which was required. The light detector was an RCA 4463 photomultiplier tube, which exhibits the bandwidth and sensitivity required for these measurements. It was installed in a Pacific Photometrics Model 76/F housing which provides for low temperature operation by cooling with dry ice to lower the noise figure and to provide improved sensitivity.

The tank used in the steady flow experiments was designed for this particular application and is shown in Figure 9. Entrance and exit windows for the laser beam were provided, and a window for observing the light scattered at an angle of 20° from the main beam was also included. The lenses and mirrors used were standard grade optical components. They performed satisfactorily since the light was monochromatic, and only a small part of the diameter of each optical component was illuminated.

There were several conditions which had to be satisfied so that the frequency shift of the laser radiation caused by Doppler effect could be observed. Since the ratio of the frequency shift to the basic frequency was very small, it was necessary to use the basic frequency as a reference to measure the amount of frequency shift. This technique is known as homodyne detection, and requires that the two beams be applied simultaneously to a nonlinear detector to recover the difference frequency. Since the photomultiplier conversion characteristics were nonlinear, it performed both functions of detection and mixing. In order to produce a useful level of difference frequency, it was necessary for the reference beam and the scattered beam to be aligned axially within a fraction of a degree, and that both wavefronts be planar. The axial alignment was accomplished visually as accurately as possible, which was sufficient to produce detectable Doppler frequency output, and final alignment was made by adjusting for maximum signal to noise ratio.

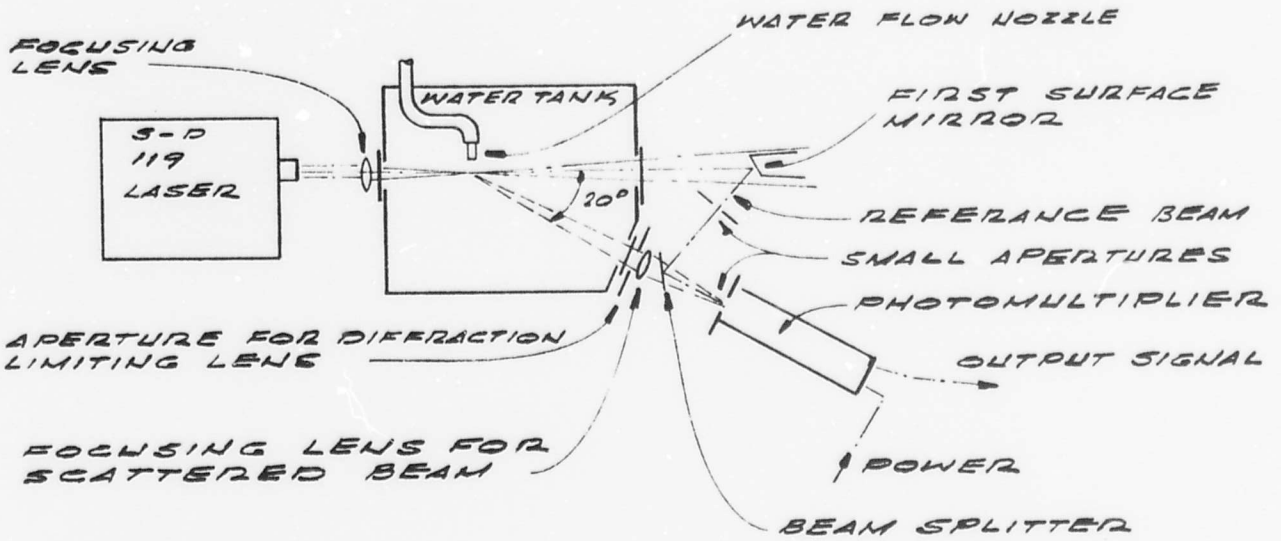

FIGURE 8. DIAGRAM OF LASER DOPPLER SYSTEM FOR MEASUREMENT OF STEADY STATE FLOW

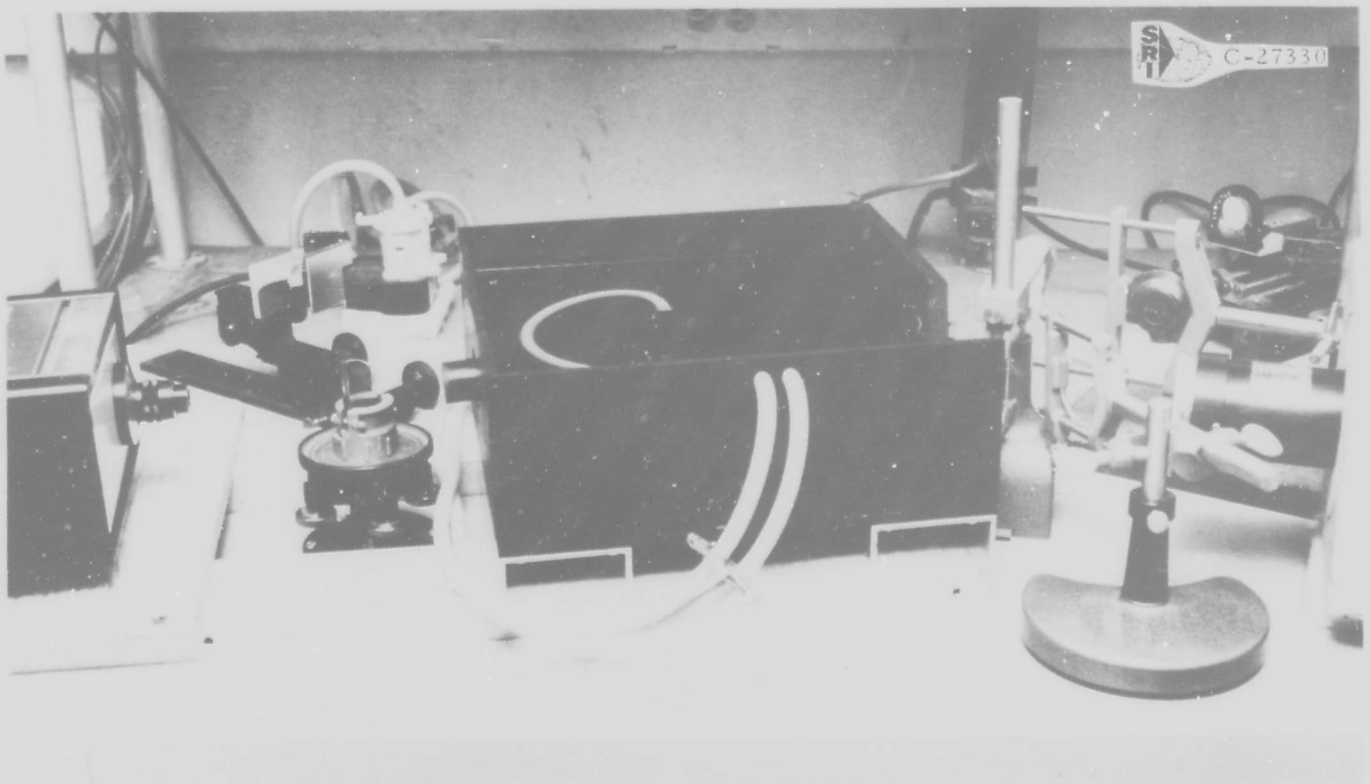

FIGURE 9. LASER, WATER TANK AND OPTICAL SYSTEM FOR STEADY FLOW MEASUREMENTS

The optical system for the scattered beam was designed to produce an image of the beam in the scattering region at the small aperture on the face of the photomultiplier assembly. The lens was diffraction limited by another aperture and adjusted to produce an Airy disk.[15] The diameter of the small aperture at the photomultiplier was constructed the size of the Airy disk.

The volume of liquid under observation by the system is defined by the intersection of a cylinder with a biconical volume. The cylinder diameter was determined by the optical system in the scattered path and was, to a first approximation, 0.005 inch. The focus of the laser beam was more difficult to define since the intensity across the beam of the focal point can be represented by a Gaussian distribution; however, in the focal zone, the useful intensity of light was within a 0.005 diameter circle. Although the volume under observation was not diminishingly small, it was considerably smaller than that occupied by any other type of pressure transducer.

Several potentially useful arrangements of light paths and optical elements were investigated, to arrive at the systems offering the best performance and stability. These variations included systems using reference beams derived directly from the laser through air paths as well as through water paths. As a result of this study, the configuration diagrammed in Figure 8 was developed. In this arrangement, the reference beam was obtained from the unscattered beam through the water filled tank. The central portion of this beam met the requirements of coherence and wavefront flatness. It was useful as a reference beam without additional optical processing. Further, the usefulness of this beam degraded very slowly with deviation from the axis since the slight misalignment of the reference beam did not reduce system performance appreciably and the Doppler effect was observable even with relatively large misalignment of the reference beam. Consequently, initial setup of the system to produce some Doppler signal was not difficult, and optimization of the system could then be performed by using the Doppler signal as an indicator.

When the system was satisfactorily aligned, measurements of Doppler frequency in relation to flow rate and direction were made. Both the magnitude and accuracy of the Doppler frequency flow measurement agreed with the magnitude and accuracy of standard methods for measuring the flow in the supply tubing. Preliminary measurements were made with an unconfined stream in the container; however, interaction of the stream anywhere in the container caused variations in flow within the scattering region. The open nozzle assembly was replaced with a 1/4 inch ID glass tube to eliminate this problem. With the tube located so that the scattering region was inside, agitation of the container caused no discernible change

in the detected Doppler signal. As a result of the small volume being observed within the flowing column, a flow profile across the diameter of the tubing could be made. A velocity ratio of about 4 to 1 was measured from the center of the stream to near the wall of the tubing under laminar (low velocity) flow conditions. With the direction of flow normal to the laser beam, the Doppler frequency varied from a few Hz to 300 kHz for flow velocities over the range of almost zero to about 60 cm/sec. This was observed over the entire range by use of a spectrum analyzer and over the low flow velocity region by audible reproduction. Figure 10 shows the effect of flow velocity on Doppler frequency. These data were obtained from 10-second exposures from a Singer-Metrics SB-7b2 spectrum analyzer. In Figure 10a the Doppler frequency for a flow velocity of 0.6 cm/sec is about 3 kHz as is indicated by the peak in amplitude at that frequency. It should be noted that the amplitude is a measure of the signal intensity at a particular frequency. It gives an indication of the number of particles moving at the velocity necessary to generate that Doppler shift frequency. The amplitude peaks at the frequency corresponding to the velocity at which the maximum number of particles are flowing. As the flow velocity was increased the peak amplitude moved to the right (Figures 10b, 10c and 10d), showing that Doppler frequency increased as the flow velocity increased. This is the result that would be expected at the highest flow rate (Figure 10d), the main flow frequency is about 28.5 kHz while a second flow frequency of importance occurs below 1 kHz. These were originally attributed to Doppler shift from heavier particles moving at a slower rate, but careful observation of the signals, in addition to data taken with the Heterodyne system (Section III. C), indicate that these spectrum analyzer responses were caused by the amplitude modulation of the signal by larger particles. This resulted from the frequency of occurrence of the particles rather than Doppler frequency caused by their velocity. In the Heterodyne system, the limiters preceding the discriminator removed such amplitude variations, and these did not appear in the output from this system. The results from steady state flow (Figure 10) are summarized as follows $\left[\psi = 90°,\ \phi = 20°\right.$ in Figure 1$\left.\right]$:

Flow Velocity (cm/sec)	Calculated Doppler Frequency (kHz)	Indicated Doppler Frequency
0.6	3	1 to 5-kHz band
2.8	14	12 to 16-kHz band
4.0	20	18 to 22-kHz band
5.7	28.5	27 to 30-kHz band

When the homodyne system was used to measure the particle velocity at the shock front produced by an underwater explosion, it was determined that the event happened too quickly to allow the Doppler shift

(a)

Low Flow Velocity
Mean Doppler Frequency ≈ 3 kHz
Mean Velocity 0.6 cm/sec

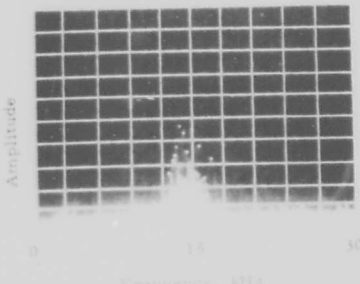

(b)

Medium Flow Velocity
Mean Doppler Frequency ≈ 14 kHz
Mean Velocity 2.8 cm/sec

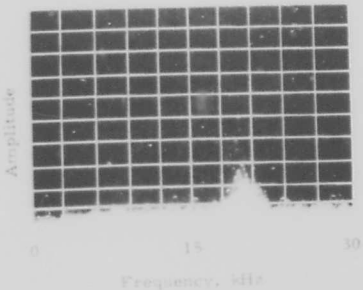

(c)

Medium Fast Flow Velocity
Mean Doppler Frequency ≈ 20 kHz
Mean Velocity 4.0 cm/sec

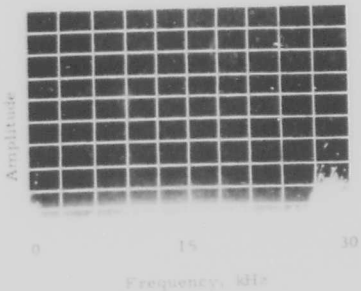

(d)

Fast Flow Velocity
Mean Doppler Frequency ≈ 28.5 kHz
Mean Velocity 5.7 cm/sec

FIGURE 10. EFFECT OF FLOW VELOCITY ON SPECTRAL DISTRIBUTION

frequency to be identified and that the signal to noise ratio with the available equipment presented formidable obstacles. Consequently, it was decided that the heterodyne system offered certain advantages.

B. Heterodyne System

The equipment used in both the Homodyne and the initial Heterodyne system was the same with the exception of the Bragg cell and the signal processing electronics. The laser was a Spectra-Physics Model 119, selected for spectral and temporal coherence as previously described. The lenses were standard optical components. The Bragg cell was constructed for this particular application, as was the water tank which contained the scattering volume. The RCA 4463 photomultiplier was selected for high quantum efficiency at 3628 Å, high amplification factor, and low drak current noise.

In the Heterodyne system, preliminary adjustments for steady flow experiments were made using a Hammarlund HQ150 receiver, which was replaced by an amplifier and discriminator chain developed specifically for this application. The initial bandwidth was 4 MHz, which was required to encompass the Doppler shift produced by the velocity ranges to be covered with the original geometry (which used $\psi = 90°$, $\phi = 20°$). The photomultiplier signal was insufficient to produce usable output from this system. By reducing the angles ψ to 5° and ϕ to 10°, the bandwidth was decreased to a magnitude of about 0.75 MHz. This reduced bandwidth enhanced the signal to noise ratio and was still compatible with the anticipated rise time of the shock front and the photomultiplier output. Since the signal to be measured was a unidirectional pulse, a predetection bandwidth of twice the signal frequency centered around the quiescent frequency was not necessary.[20]

The ultrasonic transducer used in the Bragg cell was a quartz type manufactured by Automation Industries. The nominal frequency is 30 MHz, but efficient operation on 29.5 MHz is accomplished by proper impedance matching between the driver and transducer. The driver consisted of a three-stage solid state oscillator-amplifier chain which was crystal controlled for stability. Output power was controlled by varying power supply voltage. The physical limitations of power level in the Bragg cell, as previously mentioned, precluded use of over two watts.

The detection electronics system consisted of a high-sensitivity, high-gain amplifier with a pass band from 29.5 to 33.5 MHz, followed by limiters and a discriminator. Field effect transistors were used in the input stages to provide best sensitivity, followed by integrated circuit

amplifiers and limiters. The discriminator was constructed of tuned line sections, similar in principle to Lee and Seo's system,[21] but specially designed for this application. The principal advantage of this configuration over the phase-shift, or double tuned types, is long term stability which enhances the overall system accuracy and repeatability. Several problems were encountered, including some original tendency toward instability in the amplifier due to the high overall gain required. This was eliminated by separating the amplifier into several sections to reduce possible feedback paths. Another problem encountered arose from the presence of the high power level signal at 29.5 MHz required to drive the transducer in the bragg cell, which was in close proximity to the high sensitivity amplifier tuned to the same frequency. Careful shielding and grounding reduced this interference to an insignificant level.

After the system was optimized to produce a satisfactory signal to noise ratio, the Doppler shift from particle velocity was measured by manually tuning the narrowband communications receiver to follow the change in frequency as the flow rate was varied. The signal was measured over a range of up to 100 kHz deviation from quiescent conditions, i.e., from 29.5 to 29.6 MHz. These data were taken with the same scattering geometry as in the Homodyne system ($\psi = 90°$, $\phi = 20°$):

Flow Rate (cm/sec)	Output Frequency (MHz)	Doppler Shift (kHz)
0	29.500	0
1.0	29.505	5
2.0	29.510	10
10.0	29.550	50
20.0	29.600	100

The preliminary work on the Heterodyne system was more directed at defining the operating parameters of the electronics, rather than collection of data. It was necessary to confirm that the output level of the photomultiplier was on the order of one microvolt, and that the system stability was sufficient to permit reliable Heterodyne operation. With these parameters defined, and the bandwidth considerations established, it was possible to describe the overall system geometry and the instrumentation requirements for the initial experiments on underwater detonations:

- ϕ - angle between the laser beam and the scattered beam = 10°
- ψ - angle between the laser beam and the shock propagation $0° < \psi < 20°$
- Electronic system predetection bandwidth - 750 kHz

- Electronic system postdetection bandwidth - 500 kc
- Electronic system sensitivity less than 1 microvolt

After the first few shots using parameters in the above indicated range it was evident that measurement of the particle velocity using the heterodyne system imposed several problems not encountered in measuring continuous flow velocities. The steady flow system was modified through the use of a more powerful Spectra Physics Model 122, three milliwatt laser.

A cylindrical explosive containment chamber 54" in diameter was fabricated with 1" thick plexiglass viewports, as is shown in cross section in Figure 11. The 70" high chamber was filled with water to a depth of 66". The viewports are located 34" from the bottom of the tank. The laser system was arranged around the tank in such a manner that the laser beam entered Window A and was focused through the point of measurement to exit at Window B. The laser beam passed through the tank and Window B entered the Bragg cell which produced a reference beam offset from the laser frequency by 29.5 Mc. This reference beam along with the scattered light from the measurement point were directed by the optical system to a photomultiplier tube (RCA 4463) which acted as the detector. The Window B was located to allow light scattered at an angle of 10° from the main laser beam to be utilized. The laser beam geometry and position of the explosive were selected on the basis of calculations and steady flow experiments to provide the maximum practical scattered light intensity and the minimum practical ratio of Doppler frequency shift to particle velocity. Both of these considerations were necessary to enhance the detected velocity signal to noise ratio.

Figures 12 through 14 show the laser, the optical and photomultiplier arrangement, and the tank and instrumentation. This equipment was placed in an isolated room, which could be operated as a dark room. Also, the tank was isolated from the floor by a cushion of hard rubber and plywood. The positioning table surrounding the tank was not connected to the tank and was isolated from the floor by layers of sponge rubber and plywood. A half-inch thick steel plate on the table top provided relative rigidity between the laser and detection components. This isolation was necessary since the system was sensitive enough to detect building vibration.

The photomultiplier current as well as the data from the tourmaline gages and the frequency discriminator were recorded on a magnetic tape recorder (CEC VR3300) at a speed of 60" per second. The tape was played back at a speed of 1-7/8 ips into a Honeywell Visicorder to produce visible recordings.

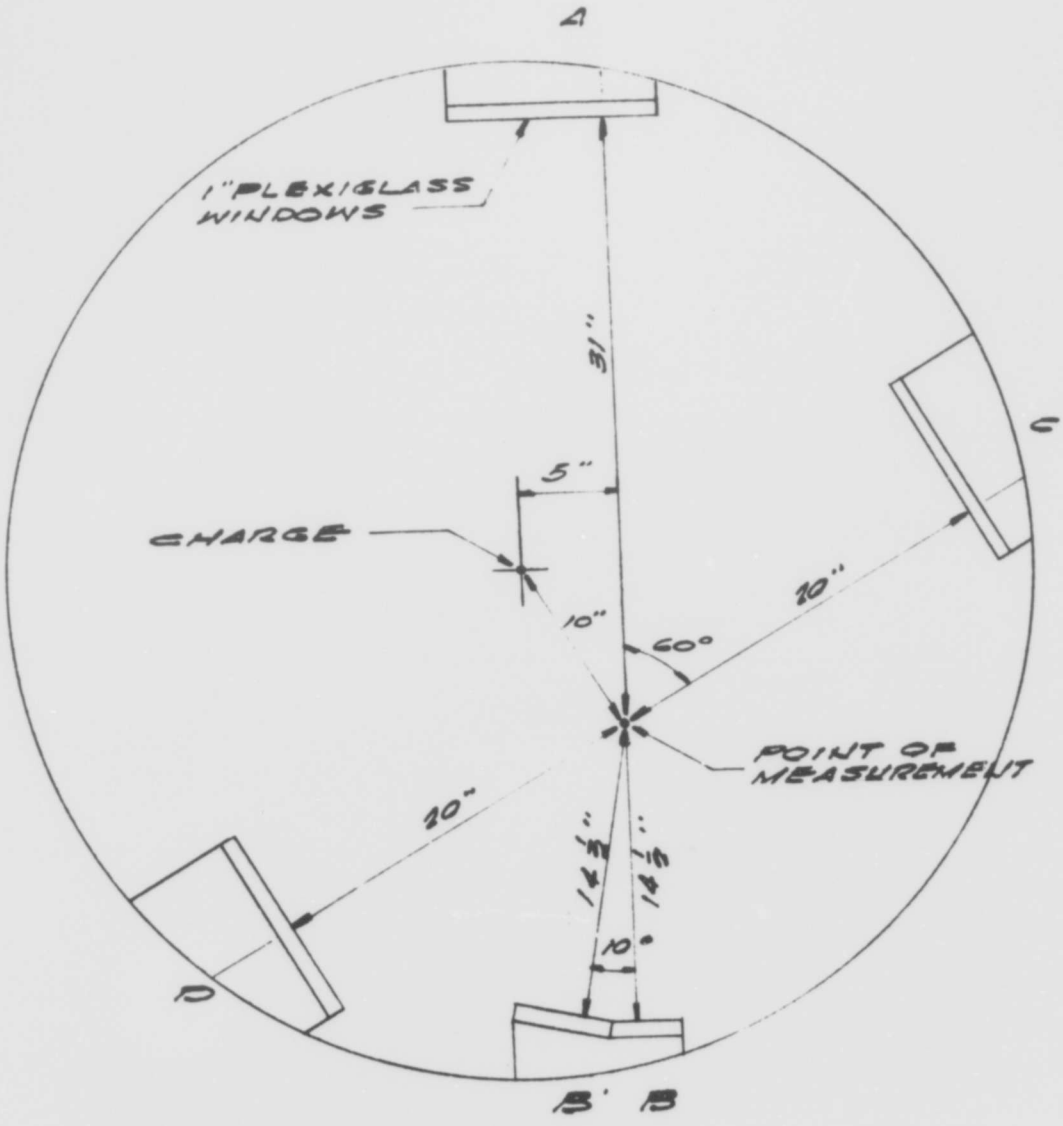

FIGURE 11. CROSS-SECTION SCHEMATIC OF EXPLOSION CONTAINMENT CHAMBER FOR INITIAL EXPLOSION TESTS

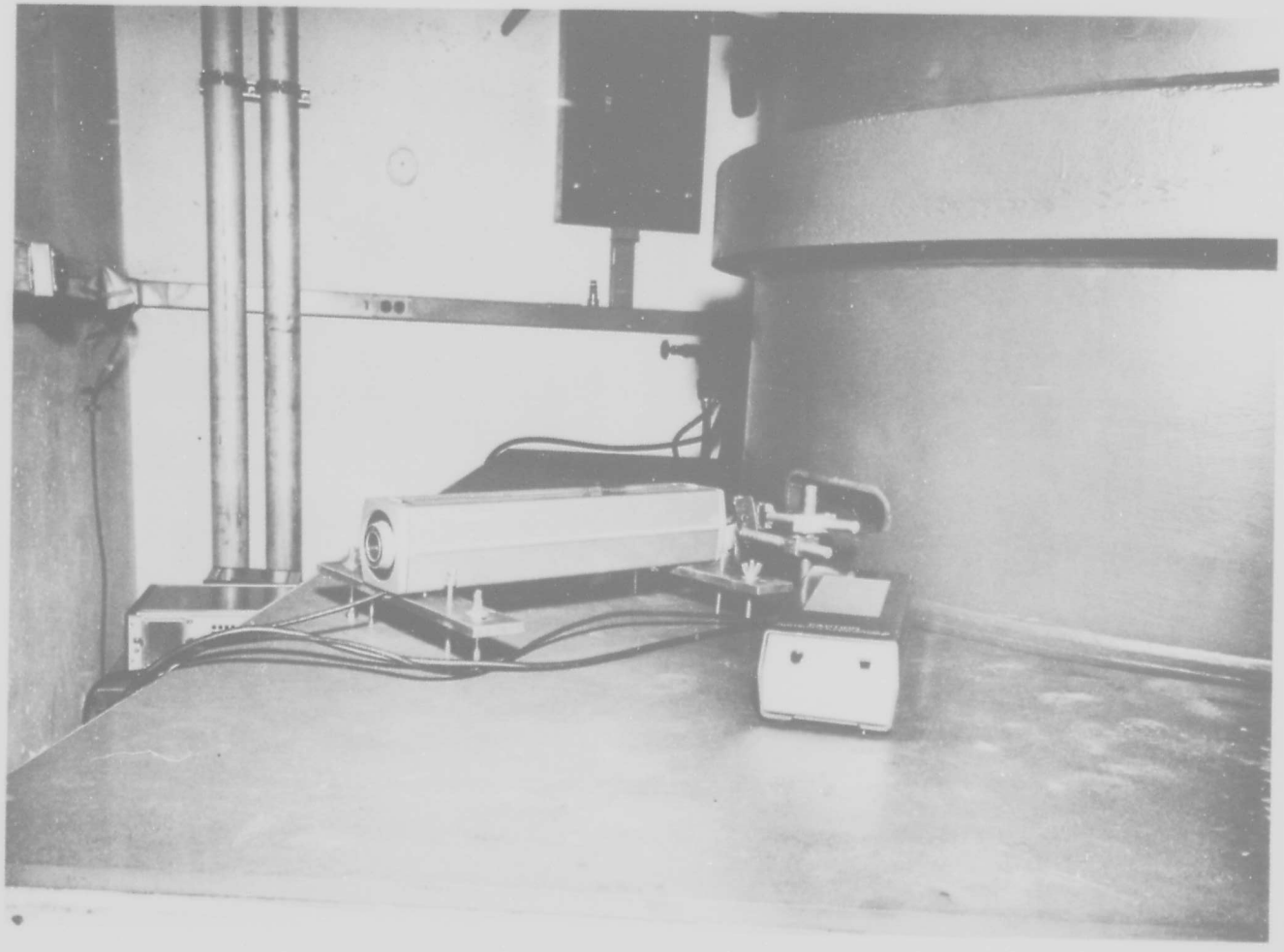

FIGURE 12 SPECTRA PHYSICS MODEL 122 LASER AND POWER SUPPLY

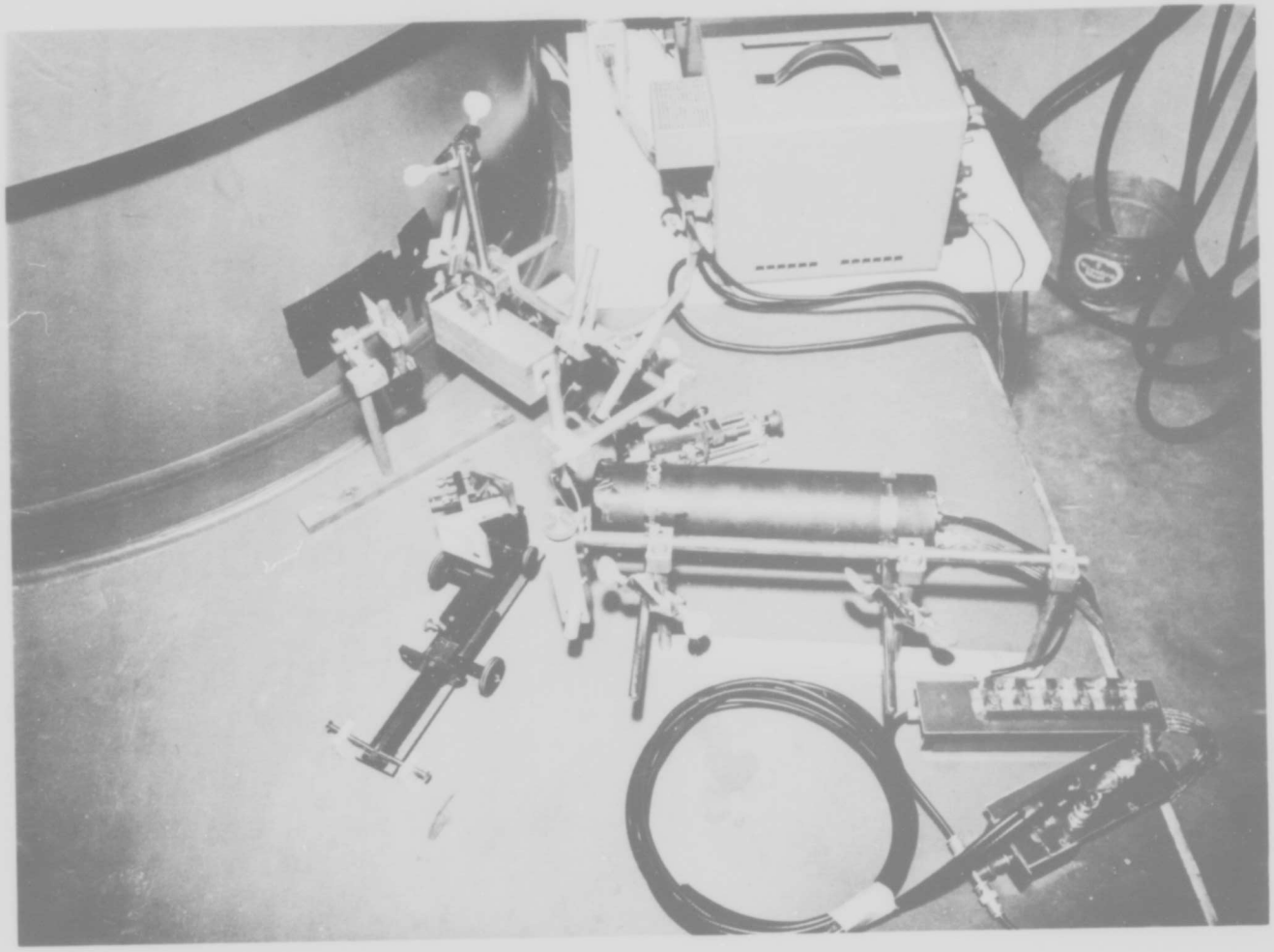

FIGURE 13. OPTICAL AND PHOTOMULTIPLIER ARRANGEMENT

FIGURE 14 EXPLOSION CONTAINMENT CHAMBER AND SIGNAL PROCESSING EQUIPMENT

Since the optimum geometry required that the photomultiplier tube be aimed toward the point of detonation, it was necessary to insure that light generated by the detonation would not interfere with the desired measurements. Figure 15 shows the output from two tourmaline pressure gages, and the photocell current, without laser excitation, during detonation. From the lower trace, it was concluded that no perceptable flash reaches the photomultiplier from the charge.

The next consideration was that the laser beam intensity remains at a usable level until after the shock front passes the point of measurement. The results of this test are shown in Figure 16, where the top two traces are again the outputs from two tourmaline gages located at the same distance from the point of detonation as the laser measurement point. The lower trace is photocell current, which is directly related to light intensity. The tourmaline gage signals show the initial shock front passage, as well as a second peak caused by the shock reflected from the wall, and returning toward the center. There was a slight loss of light intensity during the initial passage of the shock front; however, it was not great enough to cause any difficulty, and total loss of light did not occur until a considerable length of time after the initial shock front passage.

The cause for the total loss of light, which persisted for several milliseconds can possibly be explained by the bubble normally associated with underwater explosions. Figure 17 shows the same information as Figure 16, except on a compressed time scale, where the duration of the loss of signal is more apparent, and the return of light corresponds with a pressure pulse indicated by the tourmaline gages, giving added weight to the bubble explanation. Thus, in addition to confirming the availability of a useful level of laser illumination during passage of the shock front, there also appeared to be a secondary application of measuring bubble duration with the same instrumentation.

In order to separate the effects of optical phenomenon in the tank, and mechanical misalignment effects, the above tests were performed with the photocell observing the laser beam directly as it exited the tank through Window B, with a large aperture in front of the cell. To determine the possible effects of mechanical shock, the remainder of the optical system was installed and aligned, and a test made using only the reference beam, for comparison with the results of the previous test. Figure 18 shows that mechanical vibration did interfere during the time of measurement, but did cause a difference in signals after the shock had propagated into the table. This was of little concern, since it occured considerably later than the time of measurement. The third trace in Figure 18 is the output from the FM discriminator, which was included in order to determine if

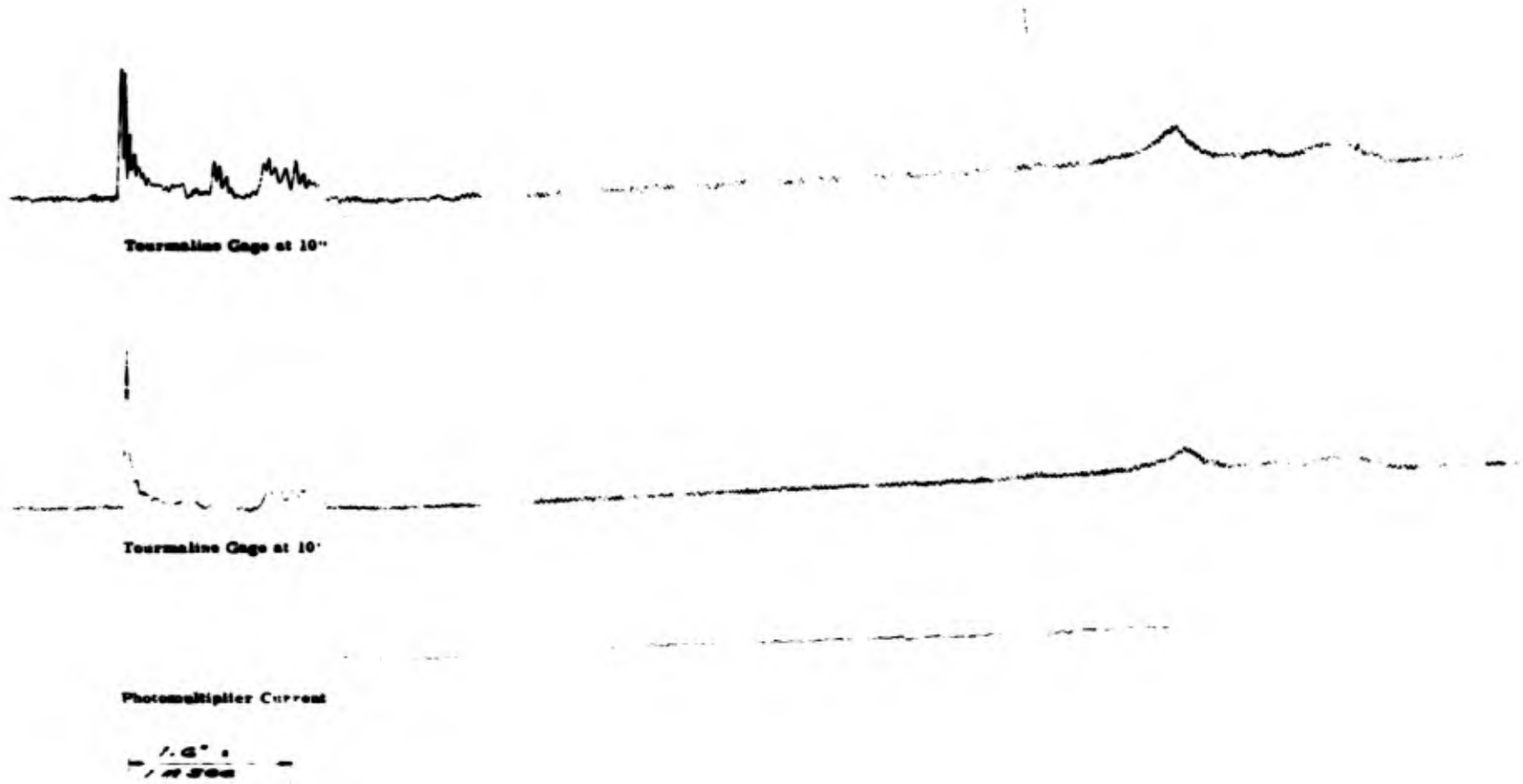

FIGURE 15. PHOTOMULTIPLIER OUTPUT WITH LASER TURNED OFF

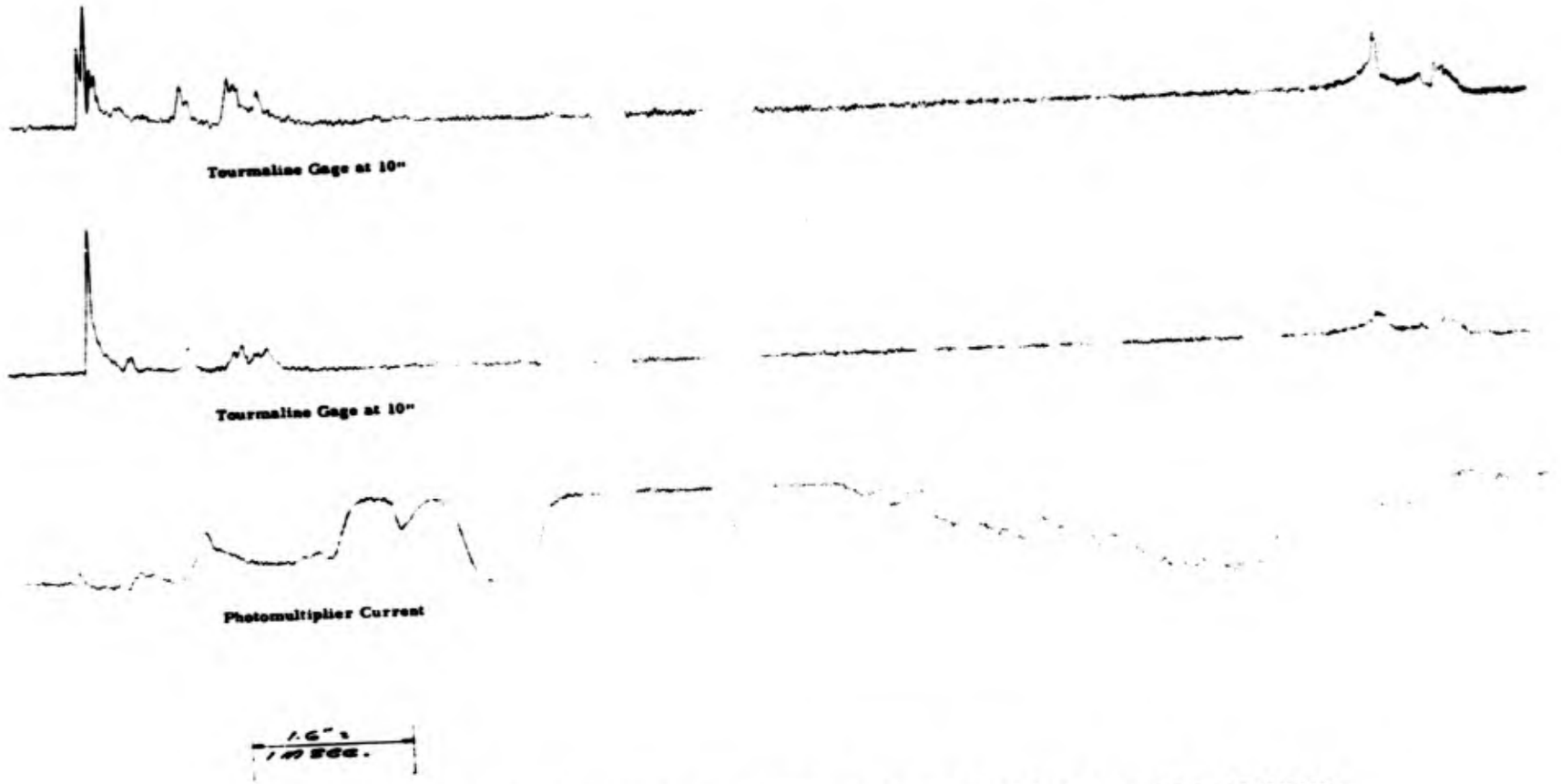

FIGURE 16. PHOTOMULTIPLIER OUTPUT WHEN AIMED AT LASER SOURCE (EXPANDED SCALE)

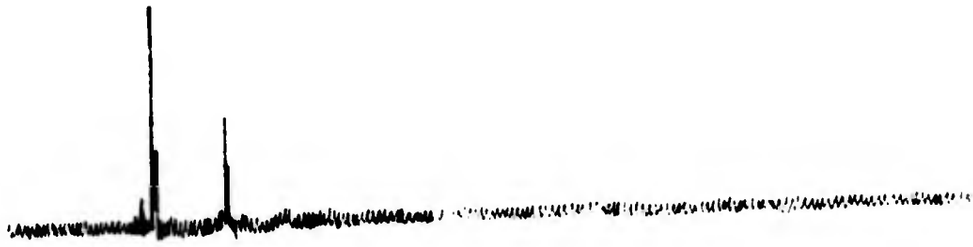

Tourmaline Gage at 10"

Tourmaline Gage at 10"

Photomultiplier Current

1.28" = 100 msec

FIGURE 17. PHOTOMULTIPLIER OUTPUT WHEN AIMED AT LASER SOURCE (COMPRESSED SCALE)

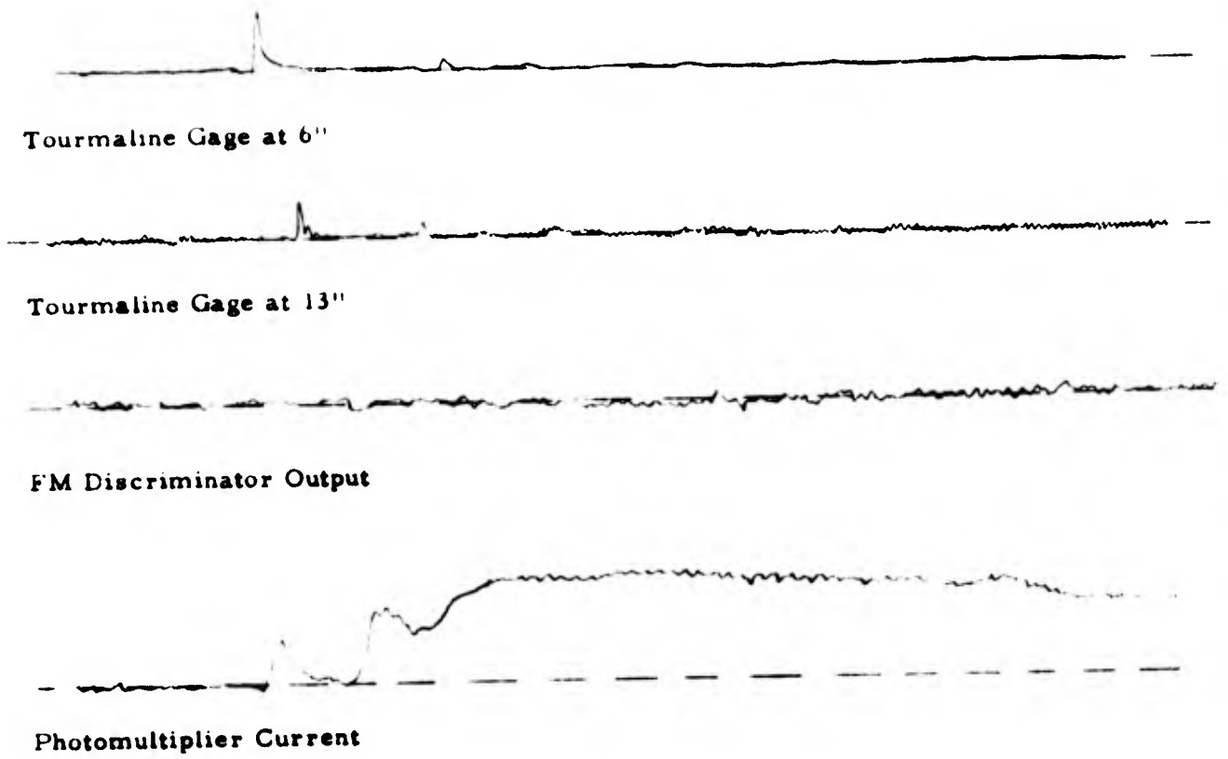

FIGURE 18. PHOTOMULTIPLIER OUTPUT FROM REFERENCE BEAM THROUGH BRAGG CELL

there were any extraneous signals produced by other mechanisms than the desired one. No output was expected, since the scattered beam, which contains the desired particle velocity Doppler information, was optically blocked for this test.

The complete optical system was then carefully aligned in order to perform Doppler shift measurements of particle velocity. Several tests were conducted using electric blasting caps in the range of 4 to 13.5 grains of RDX. Some data were obtained, but even at 13.5 grains, the signal to noise ratio was very low, as shown in Figure 19, where the FM discriminator output is the lower trace. The Doppler signal was identified by its location in time, but is not of great enough amplitude to be useful.

A test was then performed using 7.9 grams of pentolite (Figure 20), but the signal to noise ratio was still not as good as was desirable. Consequently, a Spectra Physics Model 124, 15 milliwatt laser was introduced into the system. This laser, which was used for the remainder of the tests, has a mode spacing of 214 Mhz. No interference from mode frequencies was experienced in the initial tests with the more powerful laser. Figure 21 shows a cross-section of the explosion containment chamber at the plane where the measurements were made. DuPont E99 electric blasting caps were used as the energy source and tourmaline piezoelectric gages were again used to measure the pressure at the same distance from the charge as the point of observation (Figure 21). They also provided a time reference mark for the passage of the shock front through the region of interest. Tourmaline response to shock was computed from

$$p = \frac{C}{KA} v \qquad (23)$$

where

p = shock overpressure, psi

C = capacitance in circuit, farads

KA = gage constant, coulombs/psi

v = voltage produced, volts

A schematic of the detection components is shown in Figure 22. This geometry resulted from an optimum satisfaction of several conflicting factors. It was desirable to keep the angle ϕ (Figure 22) as small as

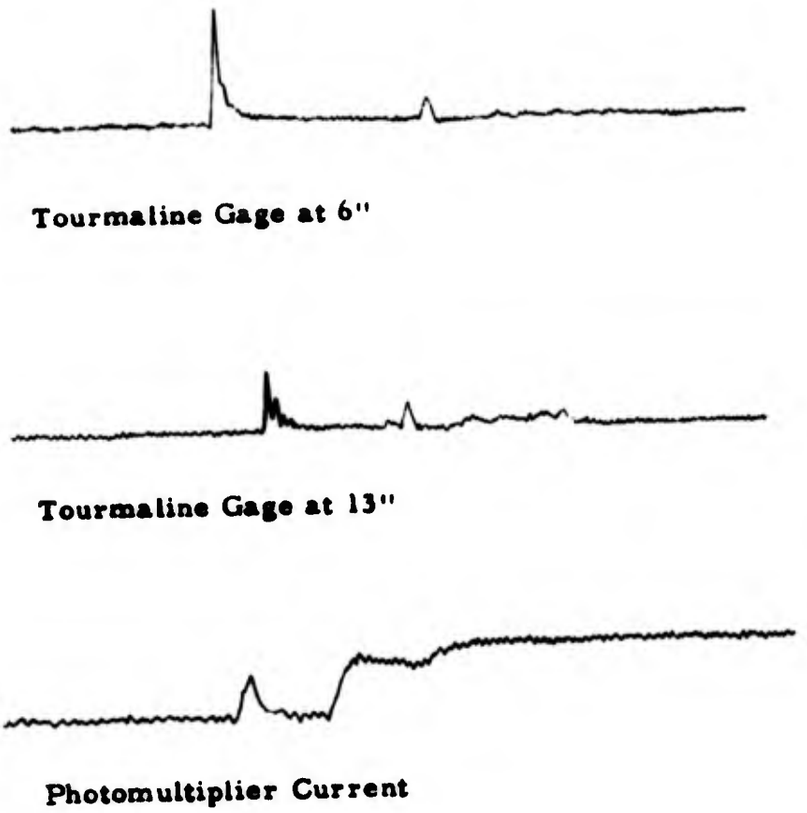

FIGURE 19. DOPPLER SHIFT FROM 13.5 GRAIN RDX EB CAP

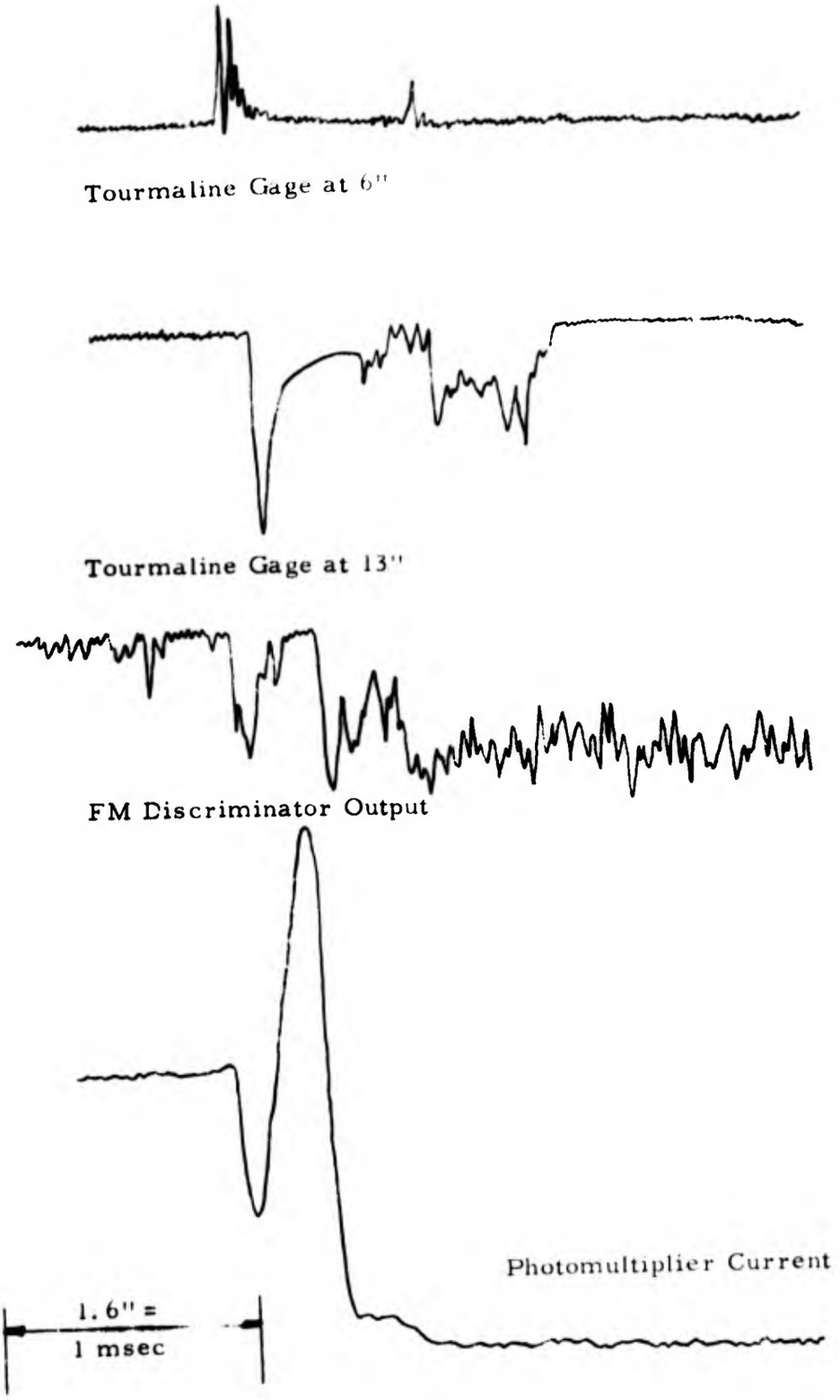

FIGURE 20. DOPPLER SHIFT FROM 7.9 GRAM PENTOLITE CHARGE

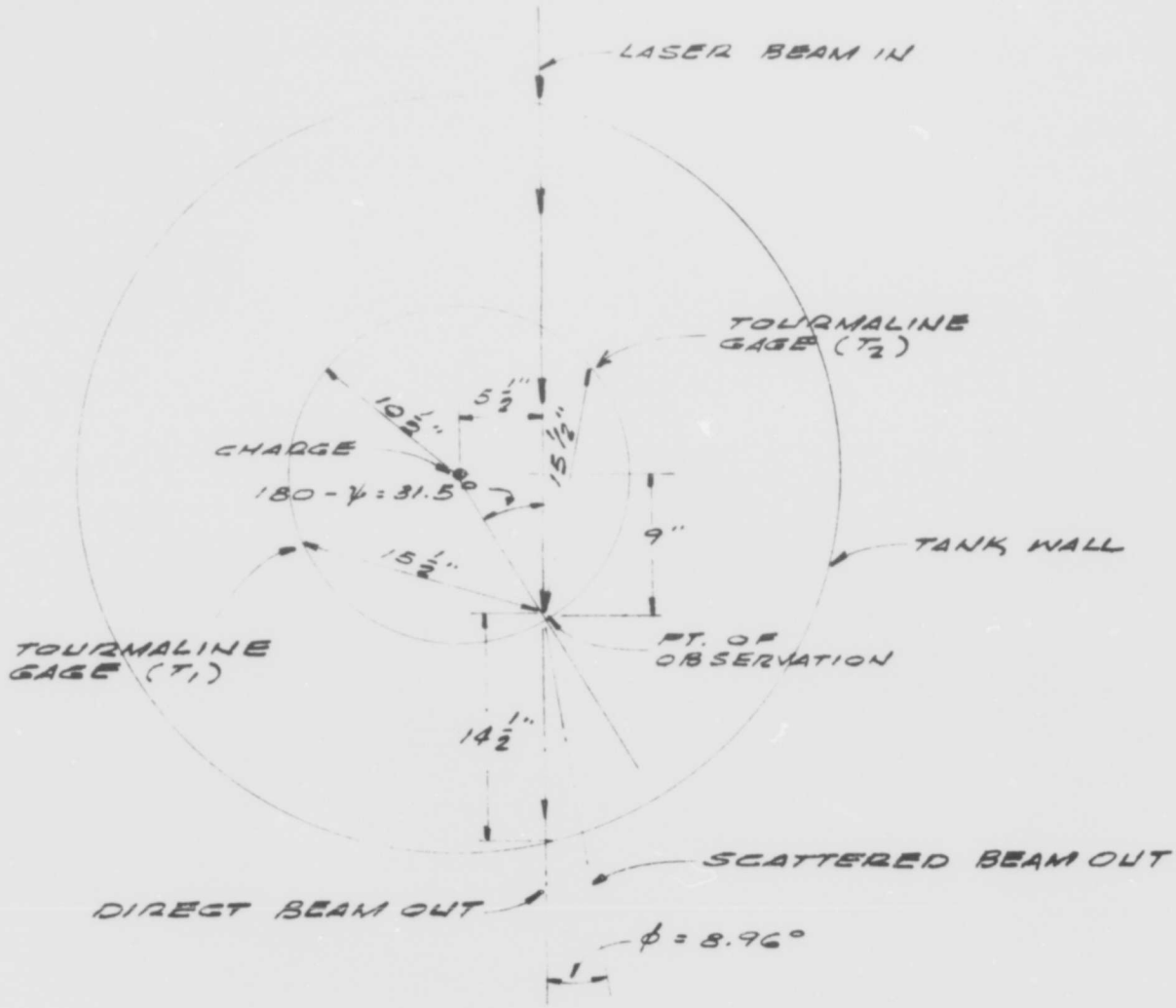

FIGURE 21. CROSS-SECTION SCHEMATIC AT VIEWPORT LEVEL

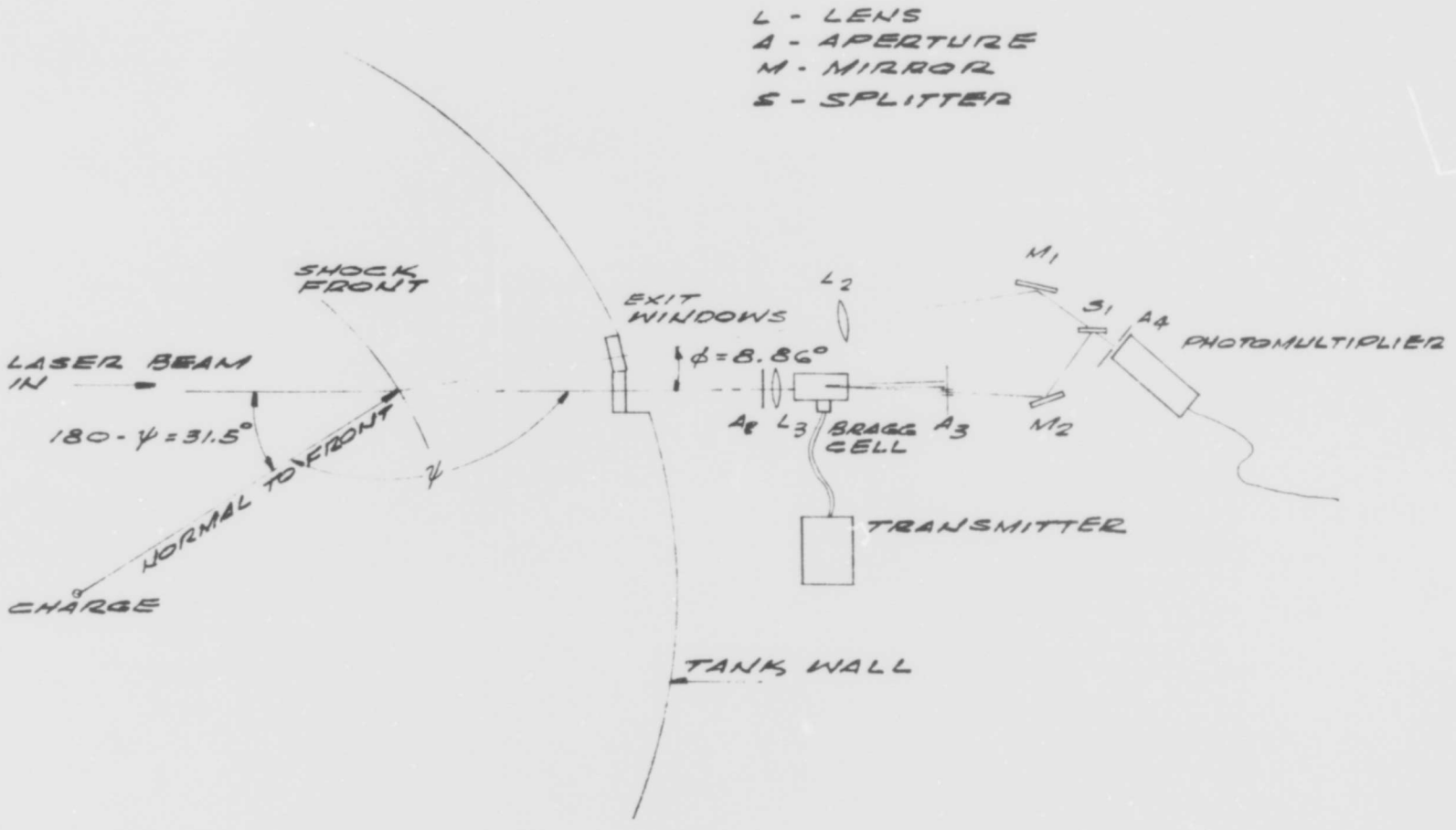

FIGURE 22. GEOMETRY OF ELECTRO-OPTICAL SYSTEM

possible in order to keep the range of the Doppler shift within the bandwidth of the electronics. On the other hand, this angle had to be large enough to keep the region under observation, which was focused on the photocathode, reasonably small. The Doppler shift is determined by Equation (7). Values of ψ and ϕ had to be such that $\Delta f \leq 750$ Kc, in order not to exceed the bandwidth of the electronics. A further constraint on the overall geometry was that the scattered path from the point of observation to the photocell must be nearly equal to the direct path plus the Bragg beam path. This was necessary to minimize signal changes caused by perterbations which affect either the common path from the laser to the point of observation, or the region between the point of observation and the photocell.

Test results are shown in Figures 23 and 24. The top two traces are shock pressure from tourmaline gages, T_1 and T_2, positioned as shown in Figure 21. The FM discriminator voltage resulted from a Doppler shift as the shock front passes the region of observation. Since this voltage is proportional to particle velocity, the shape of the curve should be similar to the response from the tourmaline gages. The bottom trace is proportional to photomultiplier current. As the region between the laser and the phototube became disturbed, the intensity of radiation received at the phototube decreased, and, as the bubble intersected the line, the output from the phototube decreased to zero. The tests shown in Figures 23 and 24 are qualitative in nature, but indicated an improvement over preliminary results in the FM discriminator signal. This was attributed to the use of a more powerful laser.

The response was still qualitative, however, due to the difficulty in focusing on a specific region. Components had to be re-aligned after each test and data that had an appropriate shape were obtained in only one shot in five. It was apparent that a tremendous improvement in signal to noise ratio was required. Analysis of the system for available means of improving signal to noise ratio indicated that the possibilities for increasing the usable signal level were: (1) a more powerful laser, (2) a reduction of light losses, (3) an increase in the ratio of scattered to incident light, (4) an increase in the solid angle over which scattered light is collected, (5) a more optimum system adjustment, and (6) a decrease in the noise level. All of these factors had been varied and optimized for the heterodyne system except for the Bragg cell.

In the heterodyne mode of operation, whereby a Bragg cell is used to generate signal offset in frequency from the main laser beam, uncontrollable scattering from the Bragg cell produces a continual signal at a Doppler frequency equivalent to a zero velocity. This extraneous signal

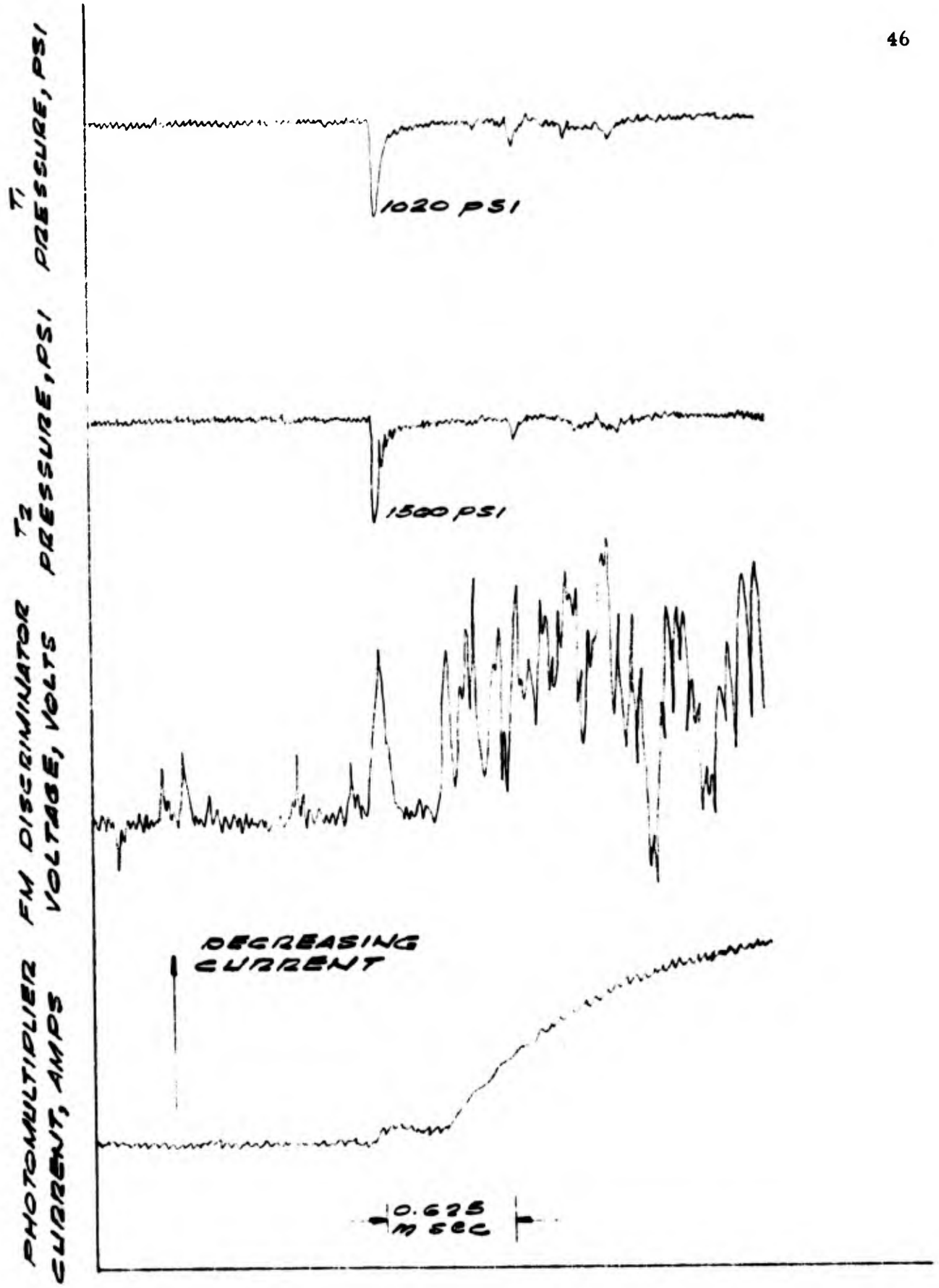

FIGURE 23. TYPICAL TEST DATA

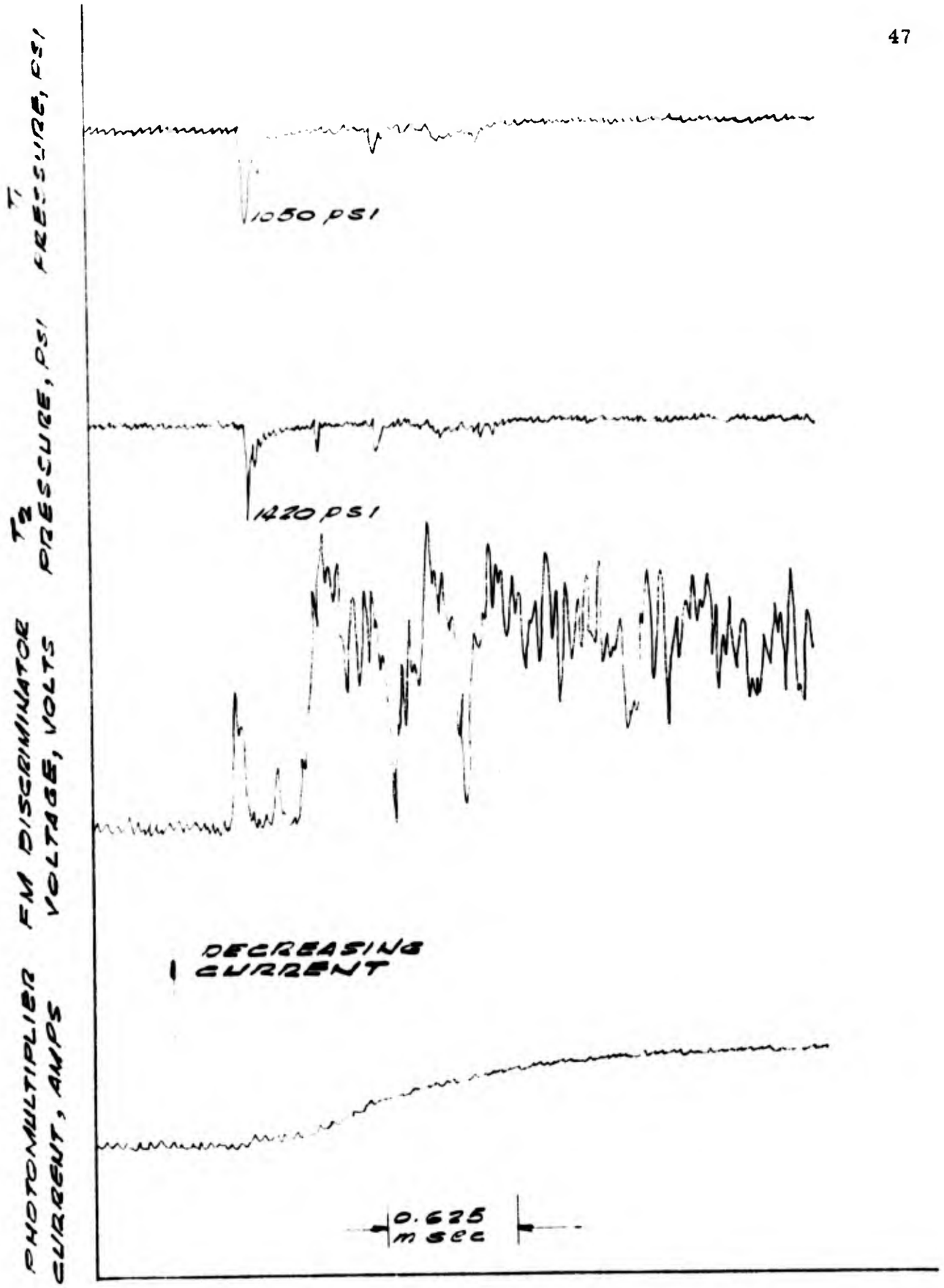

FIGURE 24. TYPICAL TEST DATA

imposes limitations on the overall dynamic capability of the FM detection electronics by masking some of the lower level Doppler signals that may be of interest. Also, it is of variable amplitude and constitutes a variable noise source. Careful alignment of the optical components diminishes this noise component considerably, but the net effect of all the noise sources in the system is to mask the signal of interest, thereby making quantitative use of the signal impossible though explosive tests consistently produce a Doppler signal when the heterodyne system is used.

Since the frequency of the single mode Model 119 Spectra Physics laser used in the initial tests of the program can be electronically controlled, an attempt was made to use it as the local oscillator in the heterodyne system, thereby getting rid of the Bragg cell. In order to accomplish this, it was necessary to force the frequency of the Model 119 laser to track as closely as possible the frequency of a single mode produced by the Model 124 laser. (The Model 124 laser has seven output modes and it was necessary in the Doppler technique being developed to use only one of these modes.) The system used to track the output mode is shown in Figure 25, but results with the system were unsuccessful. Investigations into the reason for this showed that the Model 124 laser can have frequency modulation noise of a random nature imposed on all its modes of oscillation. This noise can span as much as 10 Mhz and is critically dependent upon the cavity alignment of the laser.

C. Crossed Beam System

As an alternative to the homodyne and heterodyne systems a different system was employed in which the laser output was split into two beams, which were then focused to intersect in the region of interest. (Figures 5 and 6). The output frequency can be interpreted in terms of a particle crossing a set of fringes. Initial experiments with the split beam model were conducted in a tank in which aluminum dust was pumped at a constant rate through a glass tube in the region of interest. The Doppler signal achieved with this arrangement was sufficient to warrant the design of a system capable of being used in the explosive containment chamber. In the first system (Figure 26), the laser beam was directed onto a mirror edge so that half the beam was reflected to a second mirror. The second mirror was used to direct the reflected beam so that it would intersect the unreflected beam at the desired point. This arrangement gave maximum beam strength but was difficult to adjust, and had the disadvantage of not providing equal path lengths. These difficulties were because of small chips and geometrical irregularities on the edge of the first mirror which tended to act as light sources. Figure 27 shows the fringe pattern which was obtained with this arrangement. Close examination under a microscope shows the bright portion

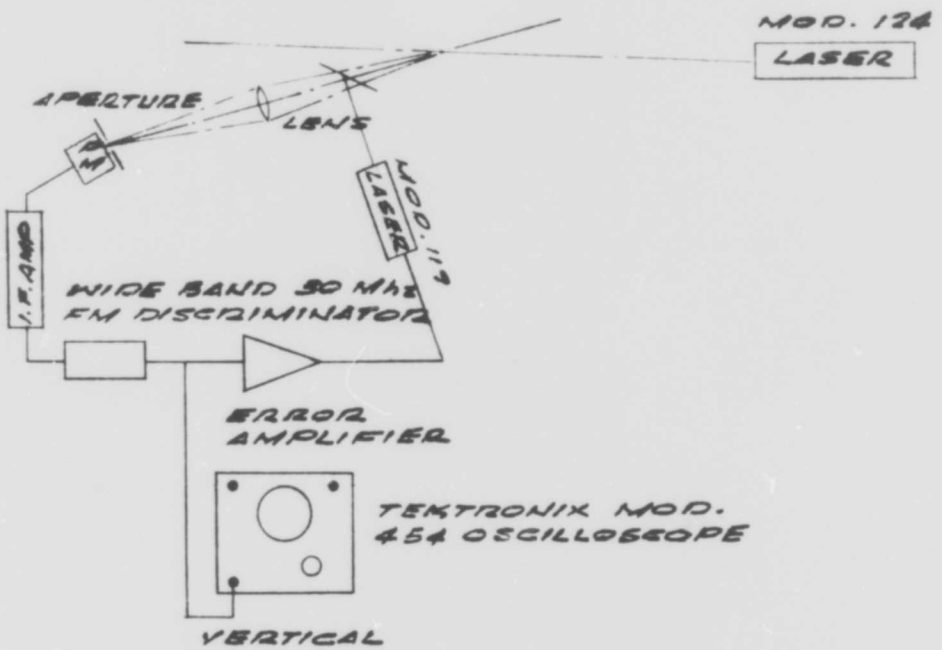

FIGURE 25. HETERODYNE SYSTEM USING MODEL 119 AS INDEPENDENT LOCAL OSCILLATOR

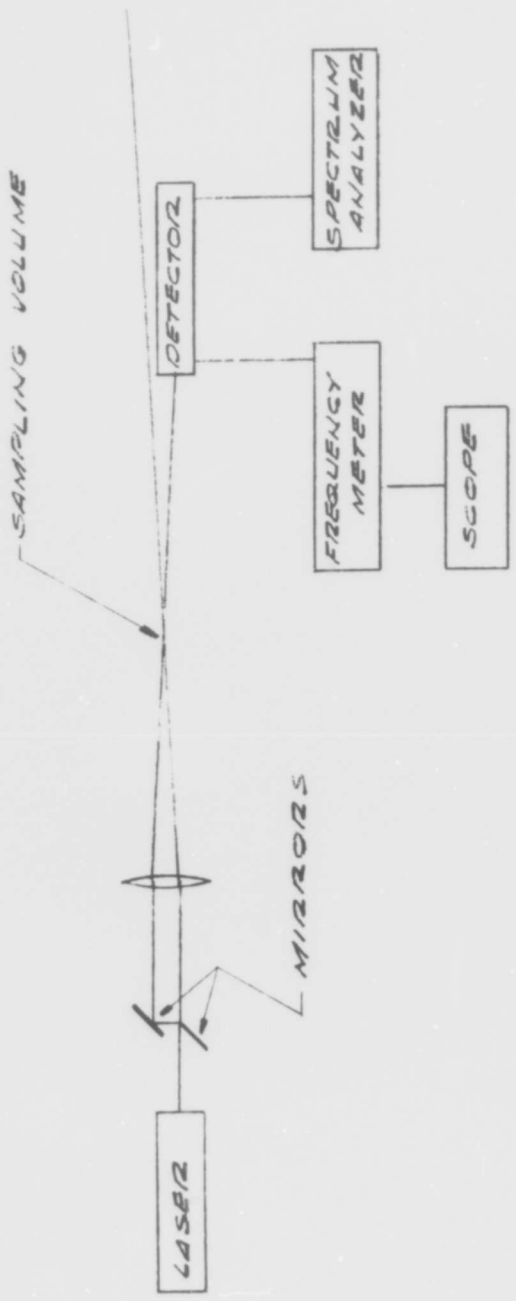

FIGURE 26. DOUBLE MIRROR ARRANGEMENT

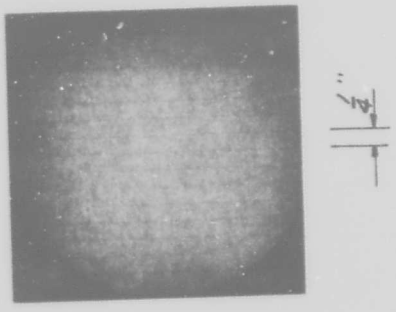

52 fringes/inch (measured under microscope)

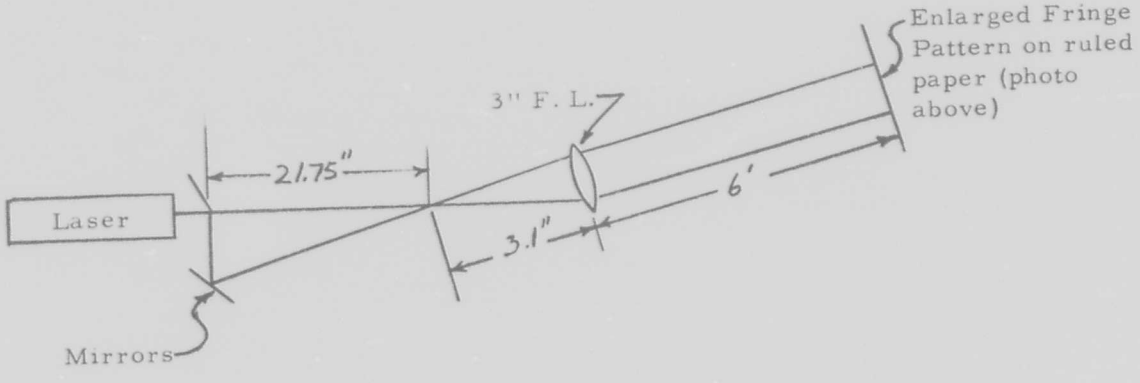

FIGURE 27. FRINGE PATTERN WITH MIRRORS

of the fringe was more than 50% of the distance between fringes. It was desirable to decrease the light portion of the fringe in order to increase the signal to noise reaching the photodetector tube.

The Doppler output as a function of beam angle for a constant particle velocity was checked by rotating a clear plastic disk, which was sprayed with 15 micron aluminum dust particles and then with lacquer, at 1,000 rpm in the region of intersection. The disk was rotated in such a way that the particles were moving at right angles to the fringes. Figure 7 shows the measured Doppler shift frequency as a function of sin α.

The most functional method for obtaining a double beam is shown in Figure 28. A diffraction grating was used to split the primary beam into several beams. By masking off the central beam and using the first order beams, it was possible to obtain a signal to noise ratio that was large relative to that obtained with previously described methods. The two first order beams, on either side of the blocked beam, were focused by the lens on the point of measurement. Second and higher order beams did not intersect the lens and were of no consequence. The angle of deviation of the first order beam from the normal to the grating is given by

$$\sin \theta = \frac{\lambda_o}{b} \tag{24}$$

where θ = angle of beam from normal
b = space between slits in grating
λ_o = wave length in air

For a 7,500 line/inch grating the angle for the first order beams is about 10.75°. Close observation of the fringe pattern obtained with this arrangement under a microscope shows that the dark and light areas are about equal. It is to be noted that the best position to observe the fringe pattern was found to be between the two beams. This permitted the fringes and shift frequency to be measured without the bright direct laser beam entering the photo tube.

Figure 29 shows the Doppler shift frequency obtained using the previously described plastic disk. The angle between the beams was 0.1 radians and the disk was rotating at 1,000 rpm. The resulting Doppler frequency was about one megacycle and had an amplitude of 0.02 volt peak to peak.

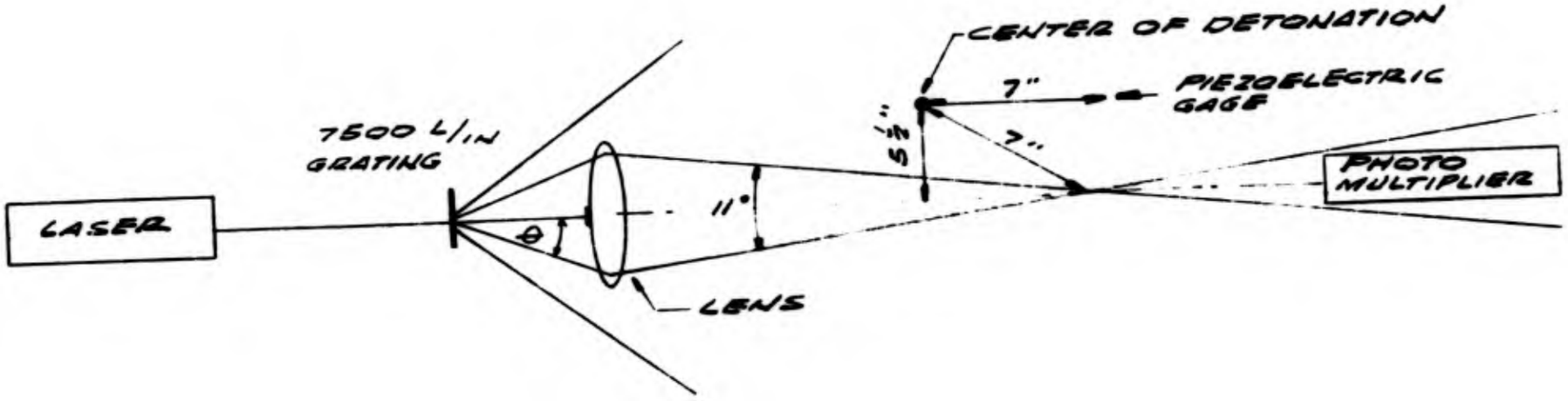

FIGURE 28. DIFFRACTION GRATING ARRANGEMENT

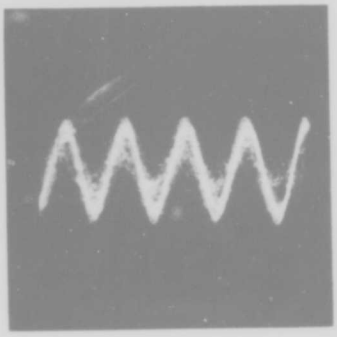

0.005 v/cm

0.5 μ sec/cm →

rpm = 1,000, 2α = 11°

radius = 1.55 inches

vel = 2π (2) (16.7) = 209 in/sec

from oscilloscope, f_d = .833 mc

from Equation (14), $\dot{u} = \frac{0.833 \times 10^{6} (249 \times 10^{-6})}{2 (.05)}$

= 207 in/sec

FIGURE 29. DOPPLER SHIFT SIGNAL FROM ROTATING WHEEL

If the Doppler frequency shown in Figure 29 results from a varying or transient particle velocity, then it would be necessary to count the peaks and determine the variation in frequency. In order to display the total pressure pulse from an underwater explosion, it is necessary to compress the time scale on the oscilloscope display. This would crowd the peaks to a point where visual counting would be dubious. Consequently, the signal from the photomultiplier tube was conditioned as shown in Figure 30 prior to being displayed on the scope. The photomultiplier tube was focused to sense only the fringe pattern. The signal from the photomultiplier was filtered so that only frequencies greater than 300 kc and less than 15 mc could be fed to a 50 ohm wide band Hewlett Packard Model 416A amplifier. Output from the amplifier was connected to a Hewlett Packard Model 521A frequency meter and discriminator. The discriminator had a sensitivity of one volt per ten Mhz. The analog output of the discriminator was band limited to 1 Mhz by means of a low pass filter. Output voltage from the discriminator was displayed on a Tektronix Model 502 dual beam oscilloscope and photographed. Figure 31 shows discriminator output for frequencies of 2, 4 and 6 megacycles obtained by rotating the plastic disk at different speeds.

After exploratory experiments, the system shown in Figure 30 was used to record pressures resulting from the detonation of electric blasting caps in the 54 inch explosive containment chamber. A 7,500 line/inch grating was positioned in front of the Spectra-Physics Model 124 He-Ne laser. The central (or zero order) beam was focused on the principal axis of a lens 3 inches in diameter with 12 cm focal length. This lens was placed 6 inches from the grating so that the two first order beams would cross about 12 inches from the lens and form an angle of 0.192 radians. The center of detonation was about 7 inches from the beam intersection and 5-1/2 inches from the principal axis of the laser (or zero order of the grating). A piezoelectric gage was also positioned 7 inches from the detonation center. One beam on the scope was used to display the discriminator output while the other beam was used to display output from the tourmaline transducer. The second beam on the oscilloscope was used to display output from a standard tourmaline piezoelectric transducer. The scope was triggered by a break wire circuit when the blasting cap detonated.

Typical results are shown in Figures 32, 33, and 34. The top trace in each figure is the response of a standard tourmaline piezoelectric gage placed 7 inches from the center of detonation, while the bottom trace is the output from the Doppler signal resulting from a fringe pattern 7 inches from the detonation point. Deflection on the bottom tract was measured beneath the pulse. In some instances the

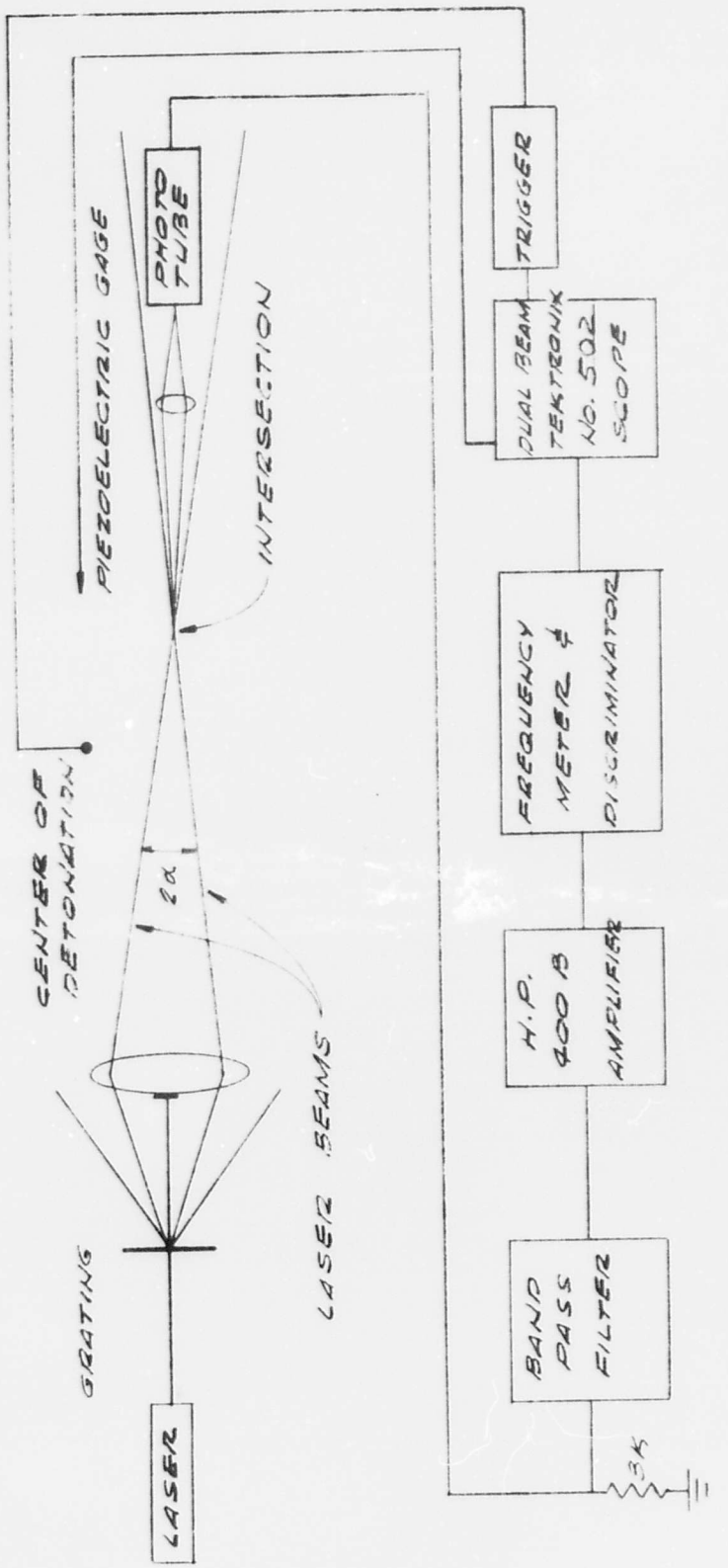

FIGURE 30. SCHEMATIC OF FRINGE SYSTEM AND SIGNAL CONDITIONING EQUIPMENT

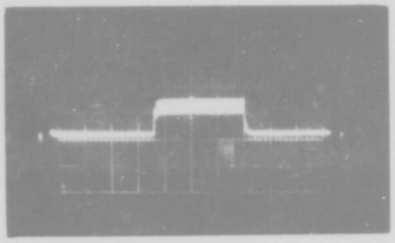

.1 VOLT/CM - 2 MC

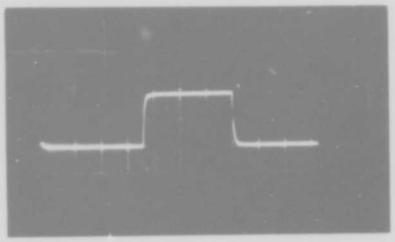

.1 VOLT/CM - 4 MC

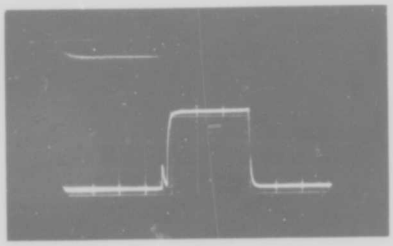

.1 VOLT/CM - 6 MC

FIGURE 31. DISCRIMINATOR OUTPUT FOR VARIOUS DOPPLER FREQUENCIES

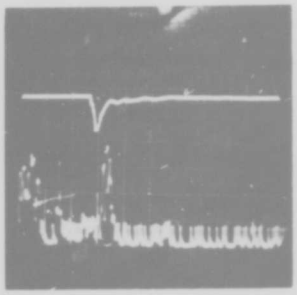

↓ .5 v/cm

↑ .2 v/cm

50 μsec/cm →

Tourmaline Gage

peak pressure = 3900 psi

Doppler System

peak deflection = 2.3 cm (beneath pulse)

f_d = 4.6 megacycles

peak pressure = 4060 psi

FIGURE 32. COMPARISON OF TOURMALINE WITH DOPPLER RESPONSE

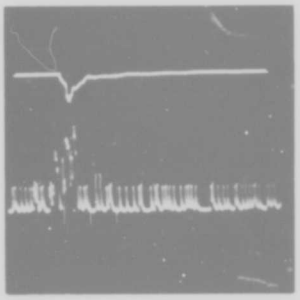

↓ .5 v/cm

↑ .2 v/cm

50 μsec/cm →

Tourmaline Gage

peak pressure = 3900 psi

Doppler System

peak deflection = 2.1 cm

f_d = 4.2 megacycles

peak pressure = 3710 psi

FIGURE 33. COMPARISON OF TOURMALINE WITH DOPPLER RESPONSE

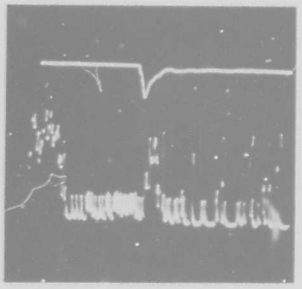

↓ .5 v/cm

↑ .2 v/cm

50 μsec/cm →

Tourmaline Gage

peak pressure = 3900 psi

Doppler System

peak deflection = 2.2 cm

f_d = 4.4 megacycles

peak pressure = 3890 psi

FIGURE 34. COMPARISON OF TOURMALINE WITH DOPPLER RESPONSE

zero line and the peak deflection are difficult to ascertain. If the bottom of the pulse is traced, the resulting curve is similar in shape to the pulse from the tourmaline gage. In each of the figures, the initial portion of the bottom trace is deflected. This initial deflection is due to light generated by the detonation.

Peak pressure as indicated by tourmaline response was calculated from Equation 23, while peak pressure indicated from the Doppler system was computed from Equation 2, with it being the value obtained by solving Equation 22 for the particle velocity.

Values shown in Figure 32 were obtained as follows:

$$\text{Tourmaline response} = 1.3 \text{ cm} \times .5 \text{ v/cm} = .65 \text{ volts}$$

$$p = \frac{.0105 \times 10^{-6}}{1.75 \times 10^{-12}} (.65) = 3,900 \text{ psi}$$

$$\text{Doppler peak deflection} = 2.3 \text{ xm} \times .2 \text{ volt/cm} = .46 \text{ volts}$$

$$f_d = \frac{.46 \text{ volts}}{.1 \text{ volt/mc}} = 4.6 \text{ megacycles}$$

$$\dot{u} = f_d \frac{\lambda_o}{2 \sin \alpha} = (4.6 \times 10^6) \frac{6.3 \times 10^{-7}}{2 \sin 5.5^\circ} \times 3.281 = 49.5 \text{ ft/sec}$$

This is the velocity perpendicular to the central laser beam. The velocity along the radius (see Figure 28) was:

$$\dot{u}_{radial} = \frac{7}{5.5} (49.5) = 63 \text{ ft/sec}$$

then $$p = 4,800 \ (1.935) \ (63) = 5850 \ \#/ft^2 = 4,060 \text{ psi}$$

Problems were encountered in obtaining particle velocity data from each test. This was due in part to the transient nature of the pulse being monitored, since the Dopplemeter system gave a consistent and adequate response from particle velocities when the fluid flow was constant or varied periodically. In earlier tests, conducted to determine the optical geometries that would produce optimum signal to noise ratios, it was found that water turbidity or particle density had a significant effect on the S/N (signal/noise) ratio when the signal resulted from a transient or shock

disturbance. Specifically, a readable signal was obtainable only in relatively clear water; after about five shots the explosion containment chamber had to be drained and refilled. Best results in signal to noise were usually obtained on the second shot in each series. Even the introduction of aluminum dust in clear water (and only at the point of observation) appeared to have an adverse effect on the S/N ratio.

Although it was evident in these early tests that water turbidity severely influenced the S/N ratio by decreasing the intensity of the beams through the water, the effect of particle size was not apparent. To determine the effect of particle size, a Holtzer-Cabot Type M synchronous motor was mounted in a welded aluminum housing. The motor shaft protruded from the housing and was sealed with a rotating water seal. Two clear plastic disks, six inches in diameter were coated with aluminum particles at the outside edge of each disk. On one disk, the particles ranged in size from .001 to .005 inch, while on the other disk they ranged from .0001 to .001 inch in size. Both disks were constructed to fit the motor shaft. This assembly was placed in the explosion containment chamber, which was filled with water. The assembly was positioned so that the ring of particles on the clear plastic disk could be rotated at the point where the split beams from the laser were focused to intersect. The direction of rotation was perpendicular to the centerline between the beams.

The plastic disks were rotated at 1,800 rpm and the particles were at a radius of 2-1/2 inches. Consequently, the velocity of particles at the point of observation was 39.2 ft/sec. In Figure 35, Doppler signal resulting from the disk with small particles is compared to the signal generalted by the disk with the large particles. For both cases, the Doppler frequency is obtained from Equation 22 with $\mathring{u} = 39.2$ ft/sec; $\sin \alpha = 0.625/12 = .052$; $\lambda_o = 6.328 \times 10^{-7}$ meters $= 2.08 \times 10^{-6}$ ft; so that the value of the Doppler frequency should be 1.96 Mhz. In Figure 35 the period of the Doppler frequency for both large and small particles is $.5 \times 10^{-6}$ sec, which corresponds to a Doppler frequency of 2.0 Mhz. From this it is seen that particle size does not affect the Doppler frequency. The signal magnitude, however, is about 25% greater for the small particles than it is for the large particles. Since the fragments and dust from several explosions would be expected to be larger than the natural particle inclusions in tap water, they would tend to decrease the signal even if they were dispersed only in the region of observation. This diminishing effect is in addition to their adverse effect on the transmission of laser energy through the water.

Several angles were used in the series of tests conducted to determine the effect of particle size on the S/N ratio. As the angle between the beams was decreased, the signal generated at the photomultiplier tube

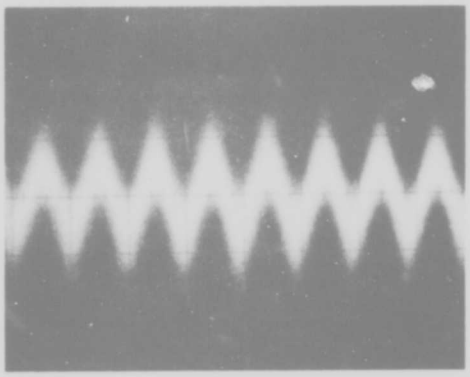

a. Large particles (.001" dia to .005" dia)

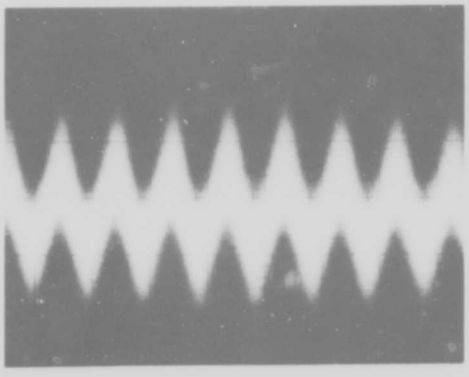

b. Small particles (.0001" dia to .001" dia)

FIGURE 35 COMPARISON OF DOPPLER SIGNAL FROM LARGE AND SMALL PARTICLES ON PLASTIC DISKS
(1800 rpm and 2.5-in. radius)

by the spinning disk became larger, with the small particles always giving a greater signal than the large particles. A series of shots were conducted with a small angle between the beams. In the first series of tests, the charge was positioned so that the shock front would become tangent to the nearer laser beam between the point of intersection and the photomultiplier tube. In early tests it was found that readable data were obtained more often when this arrangement was used. In the early tests, the optimum angle between the beams for a good S/N ratio, however, appeared to be 10 to 12 (α = 5 to 6°).

In a second series of shots, the charge was positioned 8.5 inches from the centerline so that the shock front would first become tangent to the laser beam between the laser and the point of intersection of the beams. As expected the first shot did not give readable data, but the second and third shots did give data with a readable S/N ratio, but it was not as large as was obtained with the larger angle between the beams. These data are shown in Figure 36a and 36b. In both instances the Doppler response agrees with the response from the tourmaline piezoelectric gage positioned the same distance from the charge as the point of measurement. Calculations for maximum shock overpressure are:

Tourmaline response (Figure 36a):

$$p = \frac{.0118 \times 10^{-6}}{2.02 \times 10^{-12}} \quad (.4) = \underline{\underline{2340 \text{ psi}}}$$

Doppler response (Figure 36a):

$$f_d = 0.7 \text{ cm} \times 0.2 \text{ v/cm} \times \frac{1 \text{ Mc}}{0.1} = 1.4 \text{ Mc}$$

$$\dot{u} = \frac{(1.4 \times 10^{6}) \ (2.08 \times 10^{-6})}{2(.0455)} = 31.9 \text{ ft/sec}$$

$$\dot{u}_{\text{radial}} = \frac{9.75}{8.5} \quad (31.9) = 36.6 \text{ ft/sec}$$

$$p = 4800 \text{ ft/sec} \times 1.938 \ \frac{\text{lb sec}^2}{\text{ft}^4} \times 36.6 \text{ ft/sec} = 340,000 \text{ psf}$$

$$p = 340,000 \text{ psf} \times .0069 \text{ ft}^2/\text{in}^2 = \underline{\underline{2360 \text{ psi}}}$$

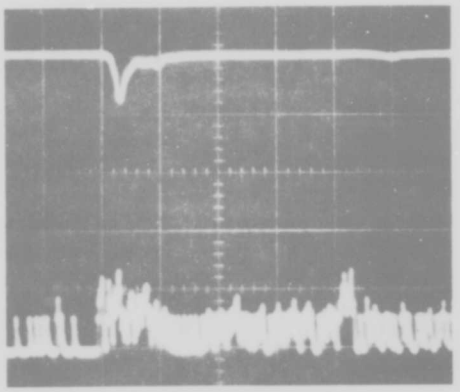

a. $\alpha = 2.6°$

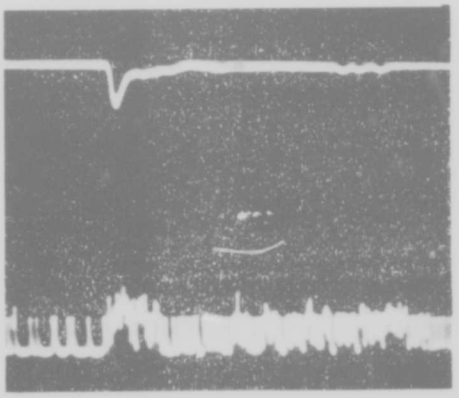

b. $\alpha = 2.47°$

FIGURE 36 COMPARISON OF TOURMALINE AND DOPPLER RESPONSE WITH POINT OF MEASUREMENT 9.75 INCHES FROM CHARGE

Tourmaline response (Figure 36b):

$$p = \frac{.0118 \times 10^{-6}}{2.02 \times 10^{-12}} (.35) = \underline{2040 \text{ psi}}$$

Doppler response (Figure 36b):

$$f_d = 0.7 \text{ cm} \times 0.2 \text{ v/cm} \times \frac{1 \text{ Mc}}{0.1} = 1.2 \text{ Mc}$$

$$\dot{u} = \frac{1.2 \times 10^{6}) (2.08 \times 10^{-6}}{2(.0433)} = 28.7 \text{ ft/sec}$$

$$\dot{u}_{\text{radial}} = \frac{9.75}{8.5} (28.7) = 32.9 \text{ ft/sec}$$

$$p = 4800 \times 1.938 \times 32.9 = 3.06 \times 10^{5} \text{ psf} = \underline{2120 \text{ psi}}$$

D. Measurement of Shock Front Velocity

After the initial tests concerned with measuring particle velocity at a shock front generated by an underwater explosion, it was apparent that a Doppler meter system could not be used to measure the shock front velocity since the front velocity was several orders of magnitude greater than the particle velocity. One straightforward technique for measuring the front velocity, involved splitting the laser beam with a double mirror arrangement so that two parallel beams 1.2 inches apart were formed. The beams were directed through the explosion containment chamber and aligned with two slits in a covering on the photomultiplier tube. The slits were 25 mils wide and 1.2 inches apart on center. The laser beams energized the photomultiplier tube by passing through the slits. A small charge was detonated 6 inches from the first beam. As the front became tangent to the first beam, a portion of the beam was reflected, decreasing the output from the photomultiplier tube. When the front became tangent to the second beam, the output was further decreased. These two sharp decreases can be seen in Figure 37.

The velocity of the shock front is given by

$$c = \frac{d}{t} \qquad (25)$$

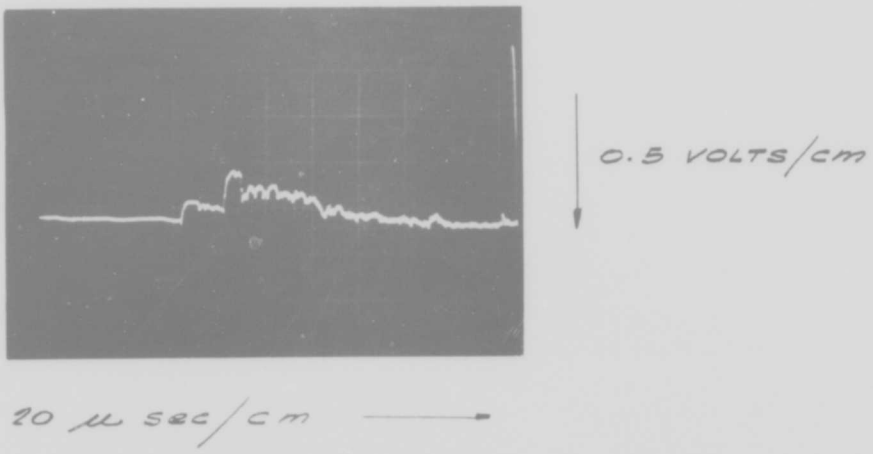

FIGURE 37. SHOCK FRONT VELOCITY AS MEASURED BY PHOTOMULTIPLIER OUTPUT

where d = distance between slits
t = time between decreases on photomultiplier output

The distance between slits would be 1.2 less .025 or 1.175 inches. From Figure 37 the time between decreases in the output from the photomultiplier tube is 20 microseconds, which gives a velocity of 4,890 feet per second, which is in agreement with the usual value of 4,000 feet per second for fresh water.

Since this arrangement could not easily be used concurrently with the Dopplermeter system, an alternate system was investigated which involved beam deflection. The laser beam was focused through the explosion containment chamber onto a viewing screen. A charge was detonated 6 inches from the laser beam. The perpendicular from the point of detonation to the laser beam was 6 feet from the viewing screen (Figure 38). A streak camera with a field of view of about 3 inches was focused on the viewing screen. The film was run at a speed of about 3000 cm/sec. In Figure 38, the distance between sprocket holes is 0.75 cm. From this, it was determined that it took the laser beam about 50 microseconds to return to its original position after it was deflected. The second deflection is due to the arrival of the bubble. This phenomenon can be explained by considering that the compression of the water due to the shock wave is sufficient to give a distinct boundary between the compressed and uncompressed region and cause the beam to be reflected when the front is tangent to the beam. From the theory of optics of thin films[22] it can be shown that

$$R_s = \frac{\mathrm{Sin}^2(\theta_o - \theta_1)}{\mathrm{Sin}^2(\theta_o + \theta_1)}, \quad R_p = \frac{\tan^2(\theta_o - \theta_1)}{\tan^2(\theta_o + \theta_1)} \tag{26}$$

where R_s is the perpendicular reflection coefficient and R_p is the parallel reflection coefficient, θ_o is the angle of incidence and θ_1 is the angle of refraction. In addition

$$n_o \mathrm{Sin}\,\theta_o = n_1 \mathrm{Sin}\,\theta_1 \tag{27}$$

when n is the refractive index for the compressed and uncompressed region. If the reflectance is plotted as a function of angle of incidence (Figure 39) it is seen that for angles of θ_o greater than about 80°, almost total reflection (or deflection) would be expected.

In addition to the high speed photographs, a photomultiplier tube with a single slit was placed with the beam just off the slit. Figure 40

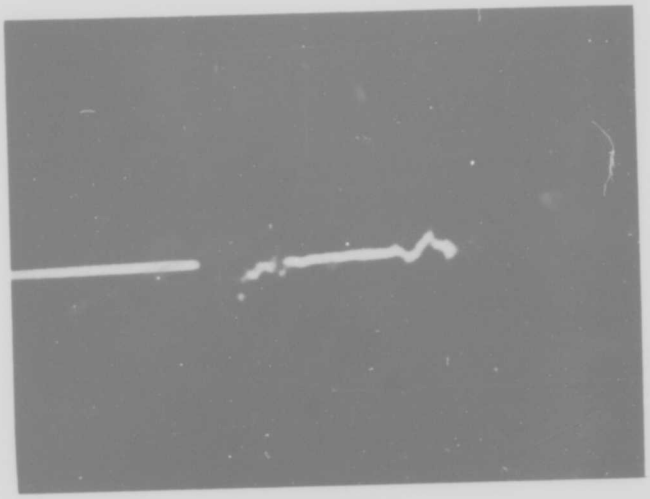

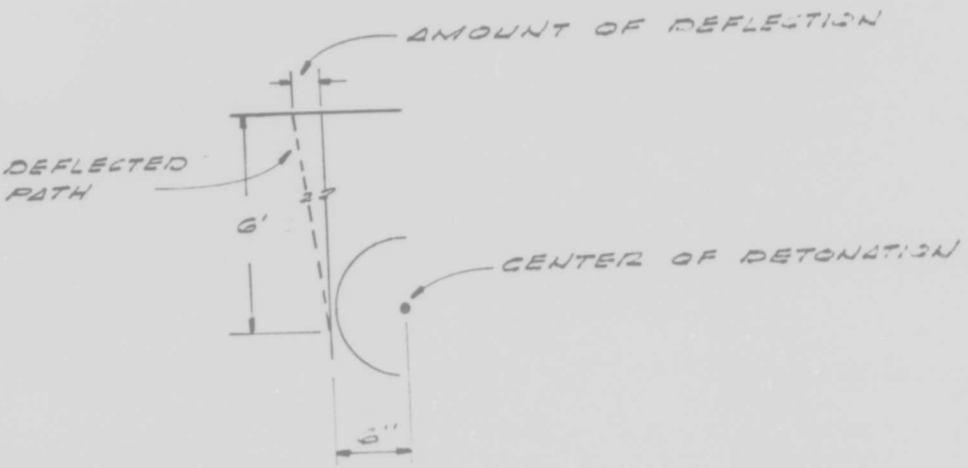

FIGURE 38. DEFLECTION OF LASER BEAM DUE TO PASSAGE OF SHOCK FRONT

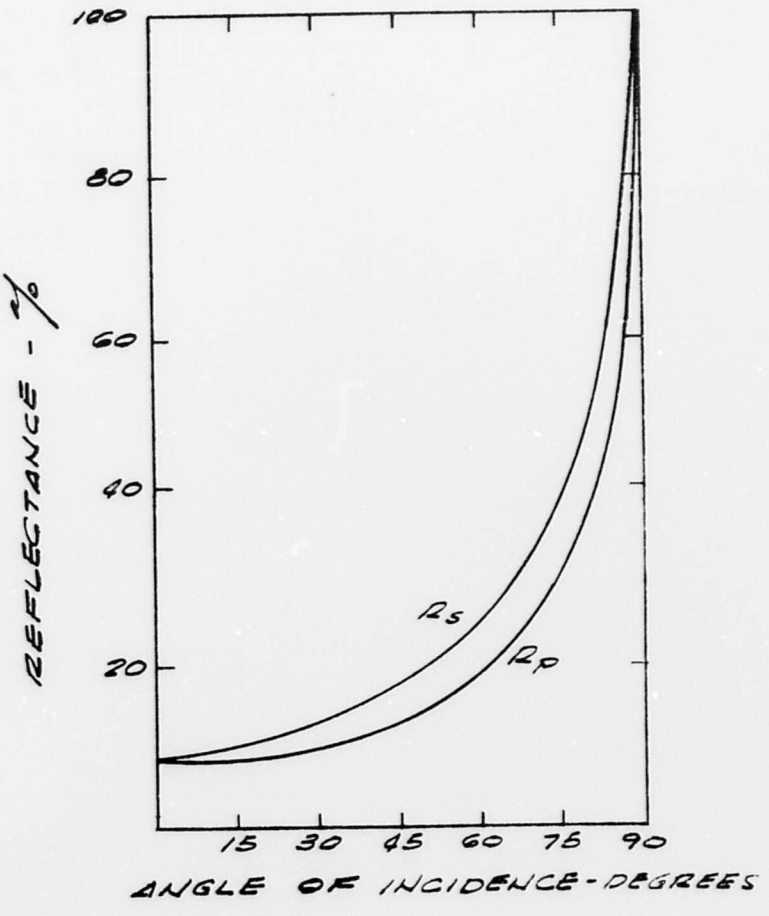

FIGURE 39. REFLECTANCE AS A FUNCTION OF ANGLE OF INCIDENCE

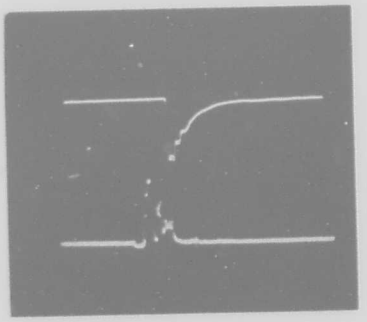

0.5 v/cm

0.2 v/cm

20 μsec/cm ⟶

Tape Trace - Tourmaline Piezoelectric Response

Bottom Trace - Photomultiplier Current

FIGURE 40. FLUCTUATION OF PHOTOMULTIPLIER CURRENT DUE TO DEFLECTION OF LASER BEAM

shows the resulting beam deflection. The photomultiplier was placed 3 feet from the charge and the charges placed 6 inches from the beam. In Figure 40 it is seen that there is first a drop in photo current. This is thought to be due to simple absorption as the front initially intersects the beam. However, destructive interference mechanisms between the reflected and unreflected portions of the beam may also be involved. As the beam is reflected further, it enters the slit and causes an increase in photomultiplier current. The beam then returns back to its original position about 40 microseconds later. This same type of deflection was noted on the crossed beam Dopplermeter system and it was necessary to place the charge so that the circular shock front emanating from the charge would not form an angle of incidence greater than 80° with either of the two beams between the laser and point of measurement at the time the front was crossing the point of measurement. It was also conceived that the rate of deflection of one of the beams would give a measurement of the shock front velocity. It would, of course, have to be calculated from the beam and charge placement geometry. Also, it required a second photomultiplier tube and such was not available.

IV. SUMMARY AND CONCLUSIONS

Three Dopplermeter systems - homodyne, heterodyne and crossed beam - were used to measure particle velocity at a shock front generated by an underwater explosion. In both the homodyne and heterodyne systems, it was not possible to achieve an acceptable signal to noise ratio. All parameters that were identified were optimized, insofar as available equipment permitted, to provide the best S/N ratio possible. Laser power was increased from 0.1 to 15 milliwatts, amplifier and photomultiplier noise was minimized, clean water and water with small foreign microparticles was used and the system geometries were optimized for minimum path length in water and maximum percentage of reflection. It was not possible to obtain a desirable signal from these systems with available equipment.

With the crossed beam system, readable results were obtained, but not in every test and further improvement in signal to noise ratio was desirable. This system, too, was optimized to the limit of available equipment. Particle velocities as measured by the Dopplermeter system agreed with the particle velocities calculated from the output of a tourmaline piezoelectric gage placed the same distance from the center of detonation as the point of measurement with the Dopplermeter.

No difficulty was encountered in measuring the shock front velocity, but a Dopplermeter system was not suitable for this purpose. The laser beam was split into two parallel beams and the time of impingement of the shock front on the two beams gave a measure of the front velocity. An investigation of laser beam deflection gave an indication that shock front velocity could be measured by timing the deflection rate of one of the beams in the crossed beam system, thereby permitting monitoring of particle and front velocities at the same time.

From the results obtained it may be concluded a crossed beam laser Dopplermeter can be used to measure particle velocity at a shock front while the shock front velocity is simultaneously monitored, which would allow for a probeless measurement of peak shock overpressure. Considering beam deflection characteristics, the method also allows for monitoring of particle velocity behind the shock front. With existing equipment, the system may be considered to be marginal, but with usual improvements in technology, it can be anticipated that the Dopplermeter system can be used to monitor transient particle velocities associated with a shock front in water.

REFERENCES

1. Cole, R. H., Underwater Explosives, (Princeton University Press, Princeton, New Jersey, 1948), pp. 35, 44.

2. Yeh, Y. and Cummins, H. Z., "Localized Fluid Flow Measurements with a He-Ne Spectrometer," Applied Physics Letters, Volume 4, No. 10, 1. 176, May 1964.

3. Foreman, J. W., George, E. W. and Lewis, R. D., "Feasibility Study of a Laser Flowmeter for Local Velocity Measurements in Gas Flow Fields," Brown Engineering Company, Technical Report No. R-149, DDC No. AD616 719.

4. Lengyel, B. A., Lasers, John Wiley & Sons, New York (1964).

5. Penndorf, R. B., "New Tables of Total Mie Scattering Coefficients for the Spherical Particles of Real Refractive Indexes," Journal Optical Society of America, Volume 47, No. 11, p. 1010, November 1957.

6. Halverson, R. R., "Theory of Peak Pressure and Time Constant Determination for Shock Waves by the Method of Optical Distortion," DDC No. AD 6841.

7. DeMaria, A. J., et al., "Ultrasonic Laser Modulation Techniques," United Aircraft Corporation, DDC No. AD 622 575, August 1965.

8. Cummins, H. Z., Knable, N. and Yeh, Y., "Observation of Diffusion Broadening of Rayleigh Scattered Light," Physical Review Letters, Volume 12, No. 6, p. 150, February 1964.

9. Foreman, J. W., George, E. W. and Lewis, R. D., "Feasibility Study of a Laser Flowmeter for Local Velocity Measurements in Gas Flow Fields," Brown Engineering Company, Technical Report No. R-149, DDC No. AD 616 719.

10. Kroeger, R. D., "Motion Sensing by Optical Heterodyne Doppler Detection from Diffuse Surfaces," Proc. IEEE, Volume 53, No. 2, p. 211, February 1965.

11. Black, H. S., Modulation Theory, D. Van Nostrand & Company, New York, pp. 37-58 (1953).

REFERENCES (CONT'D)

12. Terman, F. E., Electronic and Radio Engineering, McGraw-Hill, p. 289 (1955).

13. Adler, R., "Interaction Between Light and Sound," IEEE Spectrum, Volume 4, No. 5, pp. 42-54, May 1957.

14. Rudd, M. J., "A New Theoretical Model for the Laser Dopplermeter," J. Scientific Instrument, (J. of Physics E), Series 2, Volume 2, 1969.

15. Read, W. S. and Fried, D. L., "Optical Heterodyning with Non-Critical Angular Alignment," Proc. IRE, 51, 1987, December 1963.

16. Oliver, B. M., "Signal to Noise Ratios in Photoelectric Mixing," Proc. IRE, 49, 1960, December 1961.

17. Rabinowitz, P., Jacobs, S., Targ, R. and Gould, G., "Homodyne Detection of Phase Modulated Light," Proc. IRE, 50, 2365, November 1962.

18. Waite, T. and Gudmundsen, R. A., "A Balanced Mixer for Optical Heterodyning: The ANN Detector," Proc. IEEE, 54, 299, February 1966.

19. Waite, T., "A Balanced Mixer for Optical Heterodyning: The Magic T Optical Mixer," Proc. IEEE, 54, 334, February 1966.

20. Cuccia, C. L., Harmonics, Sidebands and Transients in Communication Engineering, McGraw-Hill, New York, p. 314 (1952).

21. Lee, C. W. and Seo, W. Y., "Super Wide-Band FM Line Discriminator," Proc. IEEE, Vol. 51, p. 1675, November 1963.

22. Van Heel, A. C. S. Advanced Optical Techniques, John Wiley and Sons, pp. 147-149, 1968.